

1 **Structural setting and fluid composition of gold mineralization along**
2 **the central segment of the Keraf suture, Neoproterozoic Nubian Shield,**
3 **Sudan: implications for the source of gold.**

4
5 Damien Gaboury¹, Hassan Nabil², Aomar Ennaciri², Lhou Maacha²

6
7 ¹ Laboratoire de Métallogénie Expérimentale et Quantitative (LAMEQ), Université du
8 Québec à Chicoutimi (UQAC), 555 Boulevard de l'Université, Chicoutimi, Québec,
9 Canada, G7H 2B1

10
11 ² Managem Mining Company (SA), Twin Center, 20330 Casablanca, Morocco

12
13
14 **ABSTRACT**

15 We provide the first large field investigation of more than 20 gold deposits and sites
16 along the Keraf suture zone, covering an area of ~15000 km². The area shows diverse
17 structural settings for gold mineralization in greenschist, amphibolite, and hornfels
18 metamorphosed rocks. The reverse fault and dyke-hosted settings appear to be the most
19 favourable for forming gold deposits. Two major N-S-trending, ~300-km-long corridors
20 of deformation are delineated (West and East) but only the West seems important for
21 gold. From fluid inclusions, 6 types of fluids are distinguished based on specific volatile
22 contents and proportions. Most types can be related to fluid evolution by hydrothermal
23 reactions and phase separations from a primitive fluid of metamorphic origin, containing
24 H₂O, CO₂, N₂, CH₄, C₂H₆, and H₂. Regional hydrothermal fields are identified based on
25 the combinations of structural settings and fluid types. The northern field is defined as a
26 single large hydrothermal system accounting for the mineralization of the 3 gold deposits
27 (WG-03, UTM and Central). For sites along the West Corridor, such as Toubi, Anas, NW
28 and Shereik, multiple and overlapping hydrothermal systems are necessary to explain the
29 various fluid types and structural settings, even at the deposit scale (Shereik). Conversely,
30 other sites (SW, Yasmine, Korup, Saijd, Dardora, Negeim, and SE) formed by localized

31 individual hydrothermal systems. The documentation of fluids containing ethane at
32 numerous sites and deposits is the most significant outcome. Such ethane-bearing fluids
33 are generated by the metamorphism of carbonaceous-pyritic sedimentary rocks. These
34 rocks are considered one of the best sources for providing ligands and gold for the
35 formation of orogenic gold deposits. Consequently, the Keraf suture zone, composed
36 mainly of carbonaceous turbidites, is interpreted to have provided such source rocks in
37 the suture zone and below the adjacent cratons during the collision, forming orogenic
38 gold deposits (graphical abstract).

39

40 **Keywords:** Orogenic Gold Deposits, Sudan, Keraf Shear Zone, Gold Source, Ethane,
41 Solid Probe Mass Spectrometry, Neoproterozoic, Structural Setting

42

43 **1. INTRODUCTION**

44 The Neoproterozoic Nubian Shield in northern Sudan is an important artisanal gold
45 production area. In 2019, Sudan produced between 120 and 200 tons (3.6 to 6.0 Moz) of
46 gold according to the Sudanese government with approximately 5 million workers in the
47 mining sector (Asharq Al-Awsat journal: 15th December 2019). Gold in the northern part
48 of Sudan has been mined since the Pharaonic period approximately 6000 years ago
49 (Klemm et al., 2001; Klemm and Klemm, 2013). Sudan is ranked third in gold production
50 for Africa behind South Africa and Ghana.

51

52 Although Sudan has a substantial gold endowment and history of Au production, modern
53 studies of gold deposits, with rare exceptions (e.g., Almond et al., 1984; Cheng et al.,
54 2017; Adam et al., 2020; Perret et al., 2020), are lacking due mostly to political
55 instability, sanctions and embargos that have restricted physical access in recent decades
56 (Trench and Groves, 2015). In contrast, hundreds of studies on gold deposits have been
57 published for the northern extension of the Nubian Shield in Egypt (e.g., Botros, 2004;
58 2004; Zoheir, 2008; Abu-Alam et al., 2018; El Aref et al., 2020;). The Sukari mine
59 (Helmy et al., 2004) in the Nubian Shield of Egypt, a 500,000 oz per year gold mine, is
60 one of the world's top-10 gold deposits (Jamasmie, 2020). In Sudan, commercial gold
61 mining is presently restricted to the Gabgaba operation by Manum, a subsidiary of the

62 Moroccan mining group MANAGEM. The Hassai gold mine, the first commercial gold
63 mine in Sudan, which produced gold from oxidized massive sulphide lenses (Barrie et al.,
64 2016), closed in 2014 after 21 years of production. Other significant gold deposits, such
65 as the Galat Sufar and nearby Wadi Doum deposits (Orca Gold), are at the development
66 stage. Another major limitation is the lack of reliable modern tectonostratigraphic
67 geological maps, although the rocks are generally well exposed in the desert.

68

69 The Neoproterozoic marks the reappearance of orogenic gold deposits, which were
70 mostly absent from 1800 to 800 Ma (Goldfarb et al., 2010; Tomkins, 2013a; Large et al.,
71 2015). This lack is interpreted as a consequence of the oxidation state of the oceans
72 (Tomkins, 2013a), where the gold in solution was at lower levels during this 1000 My
73 period (Large et al., 2015). Gold from sedimentary rocks, especially from carbonaceous
74 pyritic shales, has recently been considered the most important source for the formation
75 of orogenic gold deposits (Pitcairn et al., 2010; Large et al., 2011; Gaboury, 2013;
76 Tomkins, 2013a; Gaboury, 2019), but still remain debated for some deposits and districts
77 (Goldfarb and Groves, 2015; Wyman et al., 2016; Groves et al., 2020). The Nubian
78 Shield is thus an extraordinary natural laboratory to test whether gold deposits share the
79 same characteristics and the same sources of fluids and gold as older (Neoproterozoic and
80 Palaeoproterozoic) and younger (Palaeozoic) deposits (Gaboury, 2013).

81

82 In this paper, we describe the structural settings and styles of gold mineralization
83 occurring along the central segment of the Keraf suture, a major regional Neoproterozoic
84 suture zone. More than 20 sites have been investigated for deciphering the gold
85 mineralization contexts in an area of approximately 15 000 km². Google Earth and
86 Landsat 8 images have been used to interpret structural features and to decipher regional
87 corridors with higher potential for gold exploration. Fluid inclusions and their volatile
88 contents have been studied to document the composition of the mineralizing fluids and to
89 provide further constraints for the genetic model. Numerous orogenic mineralizing
90 systems are recorded within and proximal to the Keraf structure. Most of them are related
91 to metamorphic fluids generated by dehydration of deeper carbonaceous sedimentary

92 rocks, recognized as the most favourable sources for forming gold deposits (Gaboury,
93 2019).

94

95 **2. GEOLOGICAL SETTING**

96 The Arabian–Nubian Shield (ANS - Fig. 1) is an accretionary shield related to the Pan-
97 African orogeny that formed during convergence between East and West Gondwana from
98 ~900 to 500 Ma (e.g., El-Gaby et al., 1988; Pohl, 1988; Stern et al., 1990; Stern 1994;
99 Stern and Johnson, 2010; Johnson et al., 2011; Merdith et al., 2017). The ANS is
100 composed mainly of juvenile crustal material (Greenwood et al., 1980; Kröner et al.,
101 1987; 1992) from structurally complex assemblages of island arc, back-arc and ophiolitic
102 rocks (e.g., Teklay et al., 1998; Yibas et al., 2002; Johnson and Woldehaimanot, 2003;
103 Stern et al., 2004). The ages of the volcanic rocks and related intrusions range from 900
104 Ma to 600 Ma. Deformation, metamorphism and accretion occurred between 850 Ma and
105 500 Ma, with a peak of metamorphism and shearing occurring between 650 and 500 Ma
106 (Johnson et al., 2011, Fritz et al., 2013). The ANS has been segmented by the opening of
107 the Red Sea, which separates the Nubian Shield to the west from the Arabian Shield to
108 the east (Fig. 1). The ANS hosts numerous orogenic gold and volcanogenic massive
109 sulphide deposits (e.g., Almond et al., 1984; Botros 2002; Tadesse et al., 2003; Ghebreab
110 et al., 2009; Johnson et al., 2017). The ANS is considered the Earth’s largest gold
111 resource of the Neoproterozoic (Johnson et al., 2017).

112

113 **3. THE KERAF SUTURE ZONE**

114 The Keraf suture zone is an ~500 km-long and ~50 to 100 km-wide N-trending
115 continental arc suture (Almond and Ahmed, 1987; Stern, 1994; Abdelsalam et al., 1995,
116 Abdelsalam and Stern, 1996a; Abdelsalam et al., 1998; Bailo et al., 2003) between the
117 Neoproterozoic ANS in the east and the older East Sahara Craton to the west (Fig. 1),
118 which formed during the Neoproterozoic consolidation of Gondwana. Its interpretation as
119 a major suture zone is relatively recent: it was first recognized by Almond and Ahmed
120 (1987). The high-grade gneissic terrane to the west, referred to here as the Saharan
121 Metacraton (Abdelsalam et al., 2002; 2003), is considered pre-Neoproterozoic. It is also
122 referred to as the Nile Craton (Rocci, 1965), the Eastern Saharan Craton (Bertrand and

123 Caby, 1978), the Sahara-Congo Craton (Kröner, 1977) and the East Sahara Ghost Craton
124 (Black and Liegeois, 1993, Evuk et al., 2014; Karmakar and Schenk, 2015).

125

126 As a suture zone, Keraf is a complex belt in terms of lithologies, deformation,
127 metamorphic history and intrusive events, with variations from north to south.
128 Consequently, the physical limits of the Keraf zone are not definitive, as no authors
129 provide the same boundary and shape on their maps (e.g., Abdelsalam and Stern 1996b;
130 Bailo et al., 2003; Evuk et al., 2014; Karmakar and Schenk, 2015). As this suture zone is
131 overprinted by a late sinistral movement, it is referred to in the literature as the Keraf
132 shear zone (KSZ: Abdelsalam et al., 1995, 1998; Abdelsalam and Stern, 1996a; 1996b;
133 Abdelsalam et al., 2003). In the study area, rocks are dominated by greenschist to
134 amphibolite siliciclastic and carbonate-rich metasedimentary rocks (turbidites)
135 intercalated with sills of metabasalt and microdiorite and some pillow basaltic lavas, with
136 lesser basement windows of high- to intermediate-grade gneisses, ophiolitic nappes and
137 molasse-type sedimentary rocks cut by various types of syn- to post-tectonic intrusions
138 (Bailo et al., 2003). Bailo (2000) concluded that high-grade metamorphism occurred at
139 ~730 Ma, whereas post-tectonic plutons were emplaced as early as 710 Ma with the last
140 thermal event at 560 Ma. More recent ages for the plutonic rocks indicate that alkaline
141 magmatism occurred between 605 and 591 Ma and that later cooling continued up to 555
142 Ma (Evuk et al., 2014).

143

144 In the KSZ area, 6 deformational phases (D₁ to D₆) associated with 2 major tectonic
145 events were identified by Abdelsalam et al. (1998). D₁ and D₂ are related to the
146 emplacement of SSE-verging ophiolitic nappes due to collision between ENE-trending
147 terranes at 800-700 Ma. The E-trending Atmur-Delgo suture is the D₁-D₂ manifestation
148 and is related to the closure of an oceanic basin at approximately 750-650 Ma (Harms et
149 al., 1994; Schandelmeier et al., 1994; Abdelsalam et al., 1998, 2003). The younger
150 deformations D₃ to D₆ reflect shortening across the KSZ (Abdelsalaman et al., 1998).
151 Specifically, D₃ produced N-trending, upright, isoclinal to open folds. D₄ corresponds to
152 coaxial W-verging tight folds superimposed on D₃. D₅ refolded older structures about
153 steeply, E- to ENE-plunging fold axes. Finally, D₆ is manifested by the development of

154 local NE-trending dextral and NW-trending sinistral shear zones. The KSZ is thus
155 superimposed on E- and NE-trending D₁-D₂-related suture zones occurring on both sides
156 (Fig. 1), such as the Atmur-Delgo suture to the west and the Nakasib suture to the east
157 (Abdelsalam et al., 1995). Abdelsalam et al. (1995, 1996) proposed that the deformation
158 in the KSZ was due to sinistral transpression associated with oblique collision between
159 East and West Gondwana. The ⁴⁰Ar/³⁹Ar ages on biotite and hornblende separated from a
160 deformed granitic body indicate that the last sinistral movement along the N- and NNW-
161 trending faults took place at 580 Ma (Abdelsalam et al., 1998). According to Evuk et al.
162 (2014), post-collisional horizontal movement along the southern KSZ was probably
163 restricted to a narrow zone and occurred between 630 and 590 Ma. Therefore, the
164 sinistral transpression started at approximately 650 Ma with a terminal collision at
165 approximately 580 Ma.

166

167 **4. METHODOLOGY**

168 More than 20 gold-bearing sites and deposits, distributed in an area of 250 km (NW-SE)
169 by 100 km (SW-NE) in northern Sudan, were mapped for this study (Fig. 2). Gold
170 mineralization zones were systematically exposed by artisanal mining or by commercial
171 operation. The objective was to interpret the genetic types of these sites by characterizing
172 them in terms of the: 1) host rocks; 2) metamorphic facies; 3) hydrothermal alteration; 4)
173 structural setting; and 5) factors controlling gold mineralization. For each site, these
174 parameters were determined as far as possible, and the major structural features were
175 measured (Supp. Table SM1). The metamorphic facies were established based on the
176 occurrence of key minerals in host rocks, such as chlorite, biotite and amphibole, from
177 outcrops and thin sections. The schistosity nomenclature is as follows: S₁ is the first
178 fabric at the outcrop scale, commonly occurring as a weakly penetrative schistosity.
179 Crosscutting fabrics, named S₂ generally occur as shear zones hosting gold
180 mineralization. However, S₁ and S₂ fabrics are not necessarily correlative at the regional
181 scale, as each site is mapped according to its structural features. Planar features are
182 reported using the right-hand rule (strike/dip).

183

184 Google Earth and Landsat 8 satellite images were used to visualize the regional structural
185 features because a regional tectonic map is lacking and because the KSZ limits are not
186 well constrained (Fig. 2). The public Google Earth images have very high resolution, and
187 because there is no vegetation, outcrop features can be interpreted easily where sand
188 cover is thin. Lineaments are defined from: 1) alignment of strata; and 2) crosscutting of
189 strata. In the first case, lineaments define stratification and in the second case, structural
190 features. On the other hand, circular structures are common, clearly defining plutons.
191 Plutons are identified by: 1) the bulging of the strata around the circular edges; 2)
192 metamorphism in the hornfels facies, which has indurated the rocks and accounts for the
193 positive and dark-coloured relief; and 3) strata and foliation interrupted by circular
194 structures. Subsequently, these structures are validated and plotted precisely with the
195 Landsat 8 satellite image using MapInfo (Fig. 2).

196

197 In addition, 59 samples of gold-bearing quartz veins from all the sites and deposits were
198 collected for fluid inclusion gas analyses according to the method of Gaboury et al.
199 (2008) and Gaboury (2013). The analyses were performed at the Laboratoire de
200 métallogénie expérimentale et quantitative (LAMEQ) of the University of Quebec at
201 Chicoutimi, Canada (UQAC). Fluid inclusions in pure quartz samples of ~10 mg were
202 analysed by solid probe mass spectrometry using Stanford Research System RGA100
203 residual gas analyser (California, USA) with an electron multiplier. Ten volatiles (H₂O,
204 CO₂, N₂, C₂H₆, He, Ar, CH₄, SO₂, H₂S and H₂) were monitored in real-time during
205 progressive heating (6°C/min) up to 500°C of samples under vacuum. The raw data were
206 converted to quantitative values by background signal subtraction and correction for mass
207 interference (N₂ and CH₄). The abundance of each volatile was calculated based on
208 internal calibration parameters from the RGA100 software. Since fluid inclusion
209 decrepitations induce small pressure bursts manifested by a sawtooth signal above the
210 background, any contamination from air and other substances can be easily detected. All
211 samples were analysed at least in duplicate to ensure representativeness of the released
212 gas signal, as the fluid inclusions are not homogeneously distributed in natural samples.
213 Petrographic examination of fluid inclusions was performed on 22 selected samples to
214 characterize the fluid inclusion assemblages and to look for daughter minerals, such as

215 halite. The selection of samples for petrographic examination was based on the release of
216 a significant quantity of gas from fluid inclusion decrepitation following the solid probe
217 mass spectrometry analysis. The selection covers all the studied gold-bearing sites.

218

219 **5. REGIONAL STRUCTURAL FEATURES**

220 The interpretative tectonic map (Fig. 2) highlights two large N-S corridors defined based
221 on the alignment of lineament segments (Fig. 2) and the limits of the KSZ (Fig. 1). They
222 are referred to as the West Corridor and East Corridor. The West Corridor includes the
223 Central C02-C04 and UTM deposits and the Toubi, Shereik, Anas and NW sites (Fig. 2).
224 It thus appears to be an important corridor of deformation more than 250 km in length
225 and hosts numerous mineralized gold sites and deposits. The curved form of the corridor
226 (Fig. 2) comes from the moulding around a voluminous intrusive body according to the
227 geological map (Geological Research Authority of the Sudan, 1988 – 1/1 000 000). The
228 West Corridor corresponds to the KSZ western limit, as defined by Abdelsalam et al.
229 (1998). The East Corridor includes the SW and Yasmine mineralized sites (Fig. 2).
230 According to this interpretation, the East Corridor is continuous for approximately 300
231 km. In addition to major corridors, numerous intrusive bodies, mostly sub-circular, are
232 also delineated, ranging in size from 2 to 25 km (Fig. 2). Some of these have previously
233 been mapped and documented (e.g., Bailo et al., 2003), but most of them are newly
234 identified intrusive features.

235

236 **6. GOLD DEPOSIT STYLES AND SETTINGS**

237 Three gold deposits in the Gabgaba area, WG-03, UTM and Central, have mineral
238 resources and are studied in more detail (Supp. Table SM1; Fig. 2). WG-03 is a
239 complicated structurally-controlled gold deposit hosted in an amphibolite-facies gabbroic
240 complex (Gaboury, 2015). Gold occurs in: 1) early reverse E-W-trending shallow north-
241 dipping S_1 shear zones manifested by amphibole foliation (Fig. 3A-B); 2) N-S-trending
242 reverse sub-vertical S_2 shear zones manifested by biotite schistosity (Fig. 3B-C); and 3)
243 late centimetric extensional quartz veins oriented E-W and dipping moderately north
244 (Fig. 3D). These later veins also occur in S_1 and S_2 shear zones. The WG-03 deposit is

245 hosted close to the E-trending Atmur-Delgo suture, ~30 km from the N-trending K SZ
246 (Fig. 2).

247

248 The Central deposit includes zones C02 and C04, which are felsic dykes hosting gold-
249 bearing quartz veins (Gaboury, 2014). The felsic dykes, with thicknesses up to 15 m, are
250 oriented ~N-S with a steep dip to the E (Supp. Table SM1; Fig. 3E) and may be followed
251 for kilometres. They cut across vertical sedimentary sequences of greywacke and shales
252 having an axial planar S_1 greenschist-facies fabric (Fig. 3E). Reverse S_2 shear zones are
253 recorded at dyke contacts, and sub-horizontal extensional quartz veins are developed in
254 the competent dykes (Fig. 3E). Dykes and their host rocks record very strong iron-
255 carbonate hydrothermal alteration.

256

257 The UTM deposit, the only deposit in commercial production, corresponds to a N-S-
258 trending shallow E-dipping quartz vein system hosted in a S_2 reverse shear zone (Supp.
259 Table SM1; Fig. 3F), as indicated by CS fabrics and downdip stretching lineations
260 (Gaboury, 2014). Mineralization, as fault-fill quartz veins with metric thickness, may be
261 traced for kilometres and is developed at the contact between a large dioritic intrusion
262 and volcanic rocks in the greenschist facies. Iron carbonates and haematite dusting (Fig.
263 3F) are the main hydrothermal alterations.

264

265 **7. STYLES AND SETTING OF THE GOLD-BEARING SITES**

266 The different sites are grouped below according to the kinematics of the mineralized
267 structures (Fig. 4). This approach allows grouping of mineralization styles to better define
268 their economic potential based on geometry and lateral and vertical continuities. All gold
269 mineralization occurs as quartz veins and veinlets with very low sulphide contents (<1%)
270 and traces of muscovite (large crystals), white micas of clay size referred as sericite,
271 biotite, chlorite and carbonate minerals (Supp. Table SM2; Fig. SM1). In some cases,
272 gold is associated to the dissemination of sulphide minerals in the wall rocks.

273

274 **7.1. Reverse shearing**

275 Gold mineralization associated with reverse shearing is the most common structural
276 setting in the study area (Fig. 4). Mineralization occurs as fault-fill quartz veins
277 occupying the C plane of reverse shear zones (Fig. 5A) developed along geological
278 contacts (Fig. 5B) or dykes (Fig. 5C). These veins commonly show pinch and swell
279 geometry in cross-section and plan views, but they correspond to the veins reaching the
280 largest thicknesses locally (Fig. 5D). These structures show lateral extensions up to 700
281 m (Negeim). Iron carbonates are the main hydrothermal alteration. Mineralization is
282 hosted in S₂ high-strain zones cutting across already deformed rocks. Examples include
283 the Negeim, Yasmine West, Shereik-99 and NW sites (Supp. Table SM1).

284

285 The special case of Shereik-118, which will be a future commercial operation, is
286 noteworthy. In this specific case, the mineralization is associated with a reverse shear
287 zone, manifested by the folding of S₁ foliation (Fig. 5E). It is a ~20 m thick zone of
288 intense deformation dipping shallowly towards the west mainly (Supp. Table SM1). The
289 alteration envelope is auriferous, and the quartz and iron carbonate veins occupy the
290 hinges of centimetric to metric folds in the shear envelope (Fig. 5E).

291

292 Mineralization at WG-14 is also included in this group (Supp. Table SM1). The veins are
293 essentially hosted along an E-W-trending, shallow N-dipping S₁ high-strain zone with a
294 2-5-metre thickness (Fig. 5F). Although no kinematic indicator is observed, the geometry
295 of the veins is compatible with a compressional tectonic regime having a vertically
296 oriented σ_3 stress field.

297

298 **7.2. Strike-slip movement**

299 The gold mineralization associated with strike-slip shearing (Fig. 4), irrespective of sense
300 of movement (dextral or sinistral), is expressed by sub-vertical quartz veins. Veins are
301 thin (<30 cm) but have constant thickness with exceptional (> 1 km) lateral continuity.
302 Overall, hydrothermal alteration is very weak. The controlling factors correspond to 1)
303 mostly dyke contacts (Fig. 6A), 2) lithostratigraphic contacts (Fig. 6B), and 3) bands of
304 volcanic-sedimentary rocks (Fig. 6C). The veins are hosted in S₂ high-strain zones where
305 the intensity of deformation is typically low. It is common, especially in the volcanic-

306 sedimentary bands, to observe the S₂ trajectory deflection zone in plan view. In these
307 cases, the quartz veins are best developed as dilatant jogs within the deflections, which
308 are compatible with a strike-slip movement for providing dilation. The mineralization is
309 commonly developed as a family of parallel quartz veins. However, the spacing between
310 the veins is generally large (> 30 m). Some sites remain unclassified in terms of
311 movement sense, but they have all the attributes to classify them as strike-slip movements
312 (Supp. Table SM1). The Yasmine Principal is such a case, where a narrow quartz vein is
313 tracked over > 1 km along a dyke contact within a granitoid (Supp. Table SM1).

314

315 *7.2.1. Dextral shearing*

316 The SW sector (SW-1 and SW-2: Supp. Table SM1; Fig. 4) is a typical example of
317 dextral shearing. Numerous dykes of various compositions are intruded N-S and
318 vertically into an already deformed volcanic-sedimentary sequence (Fig. 6A). The dykes
319 cut across the S₁ fabric. The contacts of the dykes serve as S₂ shearing C planes along
320 which the veins are developed. Locally, the S fabric is developed in the dykes (Fig. 6D),
321 forming a CS relationship that confirms their dextral kinematics.

322

323 In the NW sector (Supp. Table SM1; Fig. 4), some stations expose a thin sub-vertical
324 quartz vein that appears to be better developed in the S₂ deflection compatible with a
325 dextral movement. The hydrothermal alteration of the wall rocks is characterized by
326 gold-bearing biotite, as indicated by its recovery by artisanal miners.

327

328 The Korup sector is characterized by two steeply dipping NW-SE gold-bearing S₂ high-
329 strain zones (Supp. Table SM1) spaced 30 m apart. One is developed along a volcano-
330 sedimentary horizon between massive mafic volcanic rocks (Fig. 6C). Sub-horizontal
331 stretching lineations imply a strike-slip movement. The second deformation zone
332 corresponds to an envelope of iron carbonates up to 5 m thick. Sub-vertical extensional
333 quartz veins oblique to the deformation zone and a main quartz vein parallel to the
334 carbonate envelope are developed. The geometry of the quartz vein system is coherent
335 with a dextral movement.

336

337 **7.2.2. Sinistral shearing**

338 The Dardora principal sector (Supp. Table SM1; Fig. 4) exposes all the typical
339 characteristics of gold mineralization associated with strike-slip movement. The
340 mineralization is associated with whitish quartz veins oriented N-S with sub-vertical dips.
341 Several parallel veins, spaced at least 20 m apart, are mined by artisans along a maximum
342 length of 300 m. N-S felsic dykes control the locations of veins within andesites. Along
343 the contacts between dykes and andesite, S_2 deformation zones ~1 m thick show a
344 schistosity parallel to the contacts with parallel veinlets of whitish cherty quartz <3 cm
345 thick. The only structural element for kinematic evaluation is a mined quartz vein
346 oriented at 130/90 oblique to the main N-S trend. Assuming that it was formed during
347 extension along the axis of the main NW-SE stress (σ_1), the movement along N-S dykes
348 would then have been sinistral. Similarly, deflection from N-S to NW are developed
349 along the lengths of the veins and are also compatible with a sinistral movement.

350

351 The Sajid sector is also interpreted as related to sinistral shearing (Supp. Table SM1). The
352 N-S trending sub-vertical quartz veins are developed in S_2 shear zones along lithological
353 contacts in the host sequence and some dykes. An extensional sub-vertical gold-bearing
354 vein oriented oblique to the N-S trending vein system is used as the σ_1 stress field
355 indicator for establishing the direction of movement (Fig. 6B).

356

357 **7.3. Normal Shearing**

358 Two cases of normal shearing are specifically documented, in addition to the late gold-
359 bearing quartz veins at the WG-03 deposit. These are the northern stations of the NW and
360 Shereik-118 sectors (Supp. Table SM1; Fig. 4). In the first case, CS fabrics and
361 retrograde chloritization indicate normal movement (Fig. 6E) developed along the contact
362 between massive mafic volcanic and volcano-sedimentary rocks. The mineralization
363 occurs as quartz veins in a <2 m-thick shear zone. The lateral continuity of the quartz
364 veins appears weak. For the Shereik-118 sector, the dragging of S_1 fabric at the edge of
365 the S_2 shear zone is used to establish the movement (Supp. Table SM1; Fig. 6F). The
366 mineralization takes the form of spaced (50-100 m) parallel extensional quartz veins with
367 constant thicknesses and lateral continuities over 100 m.

368

369 **7.4. Mineralized dykes**

370 This style of mineralization occurs as quartz veinlets and disseminated pyrite hosted
371 within voluminous intrusive bodies mostly occurring as dykes. These deposits are similar
372 to the mineralization of zones C02 and C04 in the Central gold deposit (Supp. Table
373 SM1). Hydrothermal alteration is manifested by iron carbonates and reddish haematite
374 dusting. The ore potential lies in the combination of the following parameters: 1) the
375 dimension of the exposed intrusive body and its continuity; 2) the intensity and diversity
376 of the quartz veinlets within the intrusive rocks; 3) the intensity of the iron carbonate
377 alteration; and 4) the presence of disseminated pyrite. From these criteria, Anas and SE
378 are the most significant sectors for this type of mineralization (Supp. Table SM1; Fig. 4).
379 This style of mineralization also occurs together with other styles in these specific
380 sectors: Shereik-118, Shereik-116, Toubi and NW (Supp. Table SM1; Fig. 4).

381

382 **8. HYDROTHERMAL ALTERATION AND METAMORPHIC FACIES**

383 The most common type of hydrothermal alteration is iron carbonates developed within
384 rocks in the greenschist facies (Supp. Table SM1; Figs. 3F, 5E-F). Sericite is locally
385 developed in quartz vein margins at the UTM and Central deposits. In the amphibolite
386 facies, biotite is the dominant mineral. Chlorite is locally developed at the margins of
387 quartz veins hosted in normal shear zones. Haematite dusting is common in intrusive
388 rocks hosting gold-bearing veinlets, such as Toubi, Dardora and SE (Supp. Table SM1,
389 Fig. SM2A-B), but this feature may be also related to surface oxidation. Aluminous
390 hydrothermal alteration, manifested by sillimanite and locally garnet, is developed in
391 mafic volcanic rocks in the Shereik area (Supp. Table SM1, Fig. SM2C-D). The
392 penetrative regional S_1 foliation at amphibolite facies is expressed by the alignment of
393 this mineral. This alteration is not related to gold mineralization and could be the result of
394 metamorphic overprint of volcanogenic-related hydrothermal alteration (Dusel-Bacon,
395 2012).

396

397 **9. MINERALIZING FLUIDS**

398 Fluid inclusions are the only direct witnesses of fluids involved in the formation of
399 hydrothermal deposits. For structurally controlled quartz-vein type gold deposits, and
400 especially orogenic gold deposits, multiple events are recorded by veins from repeated
401 fracturing and quartz precipitation (e.g., Boullier and Robert, 1992; Robert et al., 1995)
402 and even post-mineralization fluid overprint (e.g., Kerrich, 1976). Fluid inclusions can
403 also be physically modified (necked inclusions) over time (e.g., Tarantola et al., 2012). It
404 is thus fundamental, when studying fluid inclusions, to determine their genetic link with
405 gold (e.g., Wilkinson, 2001; Goldfarb and Groves 2015). Since our study is aimed at
406 providing regional characteristics, bulk volatile analysis of fluid inclusions by solid-probe
407 is considered the best approach for comparing deposits and providing constraints for
408 genetic interpretation (Guha et al., 1990). Rather than trying to link specific fluid
409 inclusions to the gold event, which may be impossible in most cases, the bulk gas
410 analysis provides an average proportion of specific gas from all the fluid inclusions.
411 This approach is also possible because numerous studies established a relatively
412 consistent ore-forming fluid through geological time (e.g., Garofalo et al., 2014; Abu-
413 Alam et al., 2018; Prokofiev and Naumov, 2020) that can be used for comparison and
414 validation of the bulk gas analyses. The petrographic documentation is also needed to
415 support the interpretation that gas is released from fluid inclusion assemblages
416 expected from vein-type gold deposits.

417

418 At a larger-scale, the direct link between gold and the analysed fluid inclusions remains
419 the weakness of any study because gold occurs at trace concentrations with an inherent
420 erratic distribution (nugget effect). To overcome this, quartz samples were only taken
421 from active stopes in artisanal operations, and in zones with gold grades for deposits at
422 exploration stage or in commercial operation. It is thus considered that the analysed
423 samples are representative of gold mineralization.

424

425 The representativeness of samples is also a major issue for any regional study and
426 especially for characterizing fluids in gold deposits. Between 2 and 6 samples were used
427 to document fluids from the various sites, depending on their known significance. As
428 stated by Ramsey and Hewitt (2005): “a representative sample is one that answers a

429 question about a population with a certain confidence.” In that sense, establishing fluid
430 types based on the bulk volatile compositions, even from a limited number of samples, is
431 considered the most representative method for addressing the fluid source and fluid
432 evolution at the regional-scale.

433

434 **9.1. Fluid inclusion gas compositions**

435 Six fluid types can be distinguished based on the contents of specific volatiles in fluid
436 inclusions and their relative proportions (Table 1, Supp. Table SM3, Fig. 7A).

437

438 Type 1 (n=19: number of samples) is aqueous-carbonic fluid, dominated by water, with a
439 complex signature including H₂O, CO₂, N₂, CH₄, C₂H₆ and ±H₂. The compositional
440 ranges are as follows (Fig. 7B): H₂O (60.3 – 95.8%), CO₂ (2.1 – 29.4%), N₂ (0.8 –
441 11.8%), CH₄ (0 – 6.5%), C₂H₆ (0.3 – 2.7%) and ±H₂ (0 – 1.5%). This fluid type is the
442 most common and is present in gold deposits at WG-03, Central, UTM and the sites at
443 Shereik, Saijd, Korup, Yasmine, Toubi and WG-14 (Fig. 7A).

444

445 Type 2 (n=4) fluids are similar to type 1 (Fig. 7) with ethane content but significantly less
446 water, having a complex signature with CO₂, N₂, CH₄, C₂H₆ and ±H₂, Ar and H₂S (Fig.
447 7A). The water proportion is below 50% (0 – 49.7%), with CO₂ (0 – 35.3%), N₂ (7.2 –
448 52.9%), CH₄ (2.6 – 30.6%), C₂H₆ (1.0 – 4.4%), H₂ (0 – 0.7%), Ar (0.17%) and H₂S
449 (0.4%) (Fig. 7B). This particular fluid type is present at NW, Dardora, Sajid and Korup.

450

451 Type 3 (n=6) is an aqueous-carbonic fluid similar to type 1 (Fig. 7), dominated by water
452 but without ethane, with proportions of H₂O (70.5 – 96.6%), CO₂ (0.4 – 15.0%), N₂ (1.2
453 – 10.4%), CH₄ (0.4 – 7.6%) and ±H₂ (0 – 1.9%). This type of fluid is documented at WG-
454 03 deposit and the sites at Shereik, Yasmine and WG-14 (Fig. 7A).

455

456 Type 4 (n=13) is an aqueous-carbonic fluid without hydrocarbons but containing nitrogen
457 and some hydrogen (Fig. 7). Their composition ranges are H₂O (64.2 – 95.8%), CO₂ (2.1
458 – 28.5%), N₂ (1.4 – 7.3%) and H₂ (0 – 1.4%). Type 4 is the only fluid documented at the
459 Negeim site. It also occurs at SW, Anas, Yasmine, WG-03, Shereik and Korup (Fig. 7A).

460

461 Type 5 (n=11) are fluids without water (Fig. 7), having variable proportions of CO₂ (0 –
462 100%), N₂ (0 – 62.8%) and CH₄ (0 – 42.4%). It is the dominant fluid at the NW site and
463 occurs at Shereik, WG-03, SE and Korup (Fig. 7A).

464

465 Finally, type 6 (n=2) is composed only of water (H₂O at 100%). It occurs only at 2 sites:
466 SE and Shereik (Fig. 7).

467

468 **9.2. Fluid inclusion petrographic characteristics**

469 Petrographic observations were performed on selected quartz samples to validate if fluid
470 inclusions can account for the released gas. Phase assemblages were established at room
471 (22°C) temperature. Quartz samples are characterized by assemblages of fluid inclusions,
472 mostly distributed as clusters and trails of secondary origin (Fig. 8) as expected for vein-
473 type gold deposits (e.g., Boullier and Robert, 1992). Fluid inclusions in all samples occur
474 in 3 distinct groups (Fig. 8): 1) translucent, two-phase liquid-vapour inclusions that have
475 water-dominated compositions and are commonly ovoid shaped with 10-30% of the
476 volume in the bubble; 2) dark, one-phase gaseous inclusions, generally ovoidal in form;
477 and 3) one-phase gaseous inclusions that are flame-shaped with darker colour. The later
478 could be partly necked inclusions from group 2. All groups have dimensions less than
479 <30 µm. For all fluid inclusion types, no daughter mineral such as halite is observed,
480 hence suggesting that the salinity of the fluids is low. Such assemblages are typical of
481 orogenic gold deposits, being composed of (1) low salinity, liquid-water inclusions with
482 bubbles of CO₂ and H₂O coexisting with (2) vapour-rich inclusions, commonly CO₂-rich
483 with variable proportions of other gas (N₂, CH₄, C₂H₆ and ±H₂, Ar and H₂S) (e.g., Ridley
484 and Diamond, 2000; Garofalo et al., 2014), resulting from pressure-induced unmixing
485 (phase separation).

486

487 In terms of fluid types, type 1 and 3 are characterized by the occurrence of the 3 groups
488 of fluid inclusions (Fig. 8). For type 2, all three groups of fluid inclusions are also
489 present, but with smaller proportions of water-dominated fluid inclusions of group 1.

490 Type 4 is also indistinguishable from types 1 and 3, being composed of the 3 groups of

491 fluid inclusions. Type 5, which is devoid of water, is dominated by gaseous fluid
492 inclusions of groups 2 and 3. Simply, the observed proportion of the 3 groups of fluid
493 inclusions (Fig. 8) is consistent with the percentage of gas and water released by
494 decrepitations (Fig. 7) and used for establishing fluid types. Consequently, the vapour-
495 rich fluid inclusions of groups 2 and 3 are carrying most of all the gaseous species (N₂,
496 CO₂, H₂, CH₄, and C₂H₆) of the fluid types 1 to 5. This is a validation that the defined
497 fluid types are well-represented by fluid inclusion groups, which are also consistent with
498 what is expected for gold deposits. The genetic implications between fluid types and fluid
499 inclusions are discussed below.

500

501 **9.3. Link between fluid type and structural setting**

502 Fluid types are compared to structural settings (Fig. 9A) and metamorphic facies (Fig.
503 9B). For the structural setting, some relationships between structural setting and fluid
504 types can be established. For reverse kinematics, including reverse-oblique movements,
505 which are the most common settings for gold-bearing quartz veins, type 1 fluid is
506 dominant (20% of the database), with smaller proportions of types 4 (14%) and 3 (8%).
507 For quartz veins hosted in normal shear zones, water-devoid type 5 is dominant (8%). For
508 dextral, sinistral and strike-slip settings, no clear dominance of fluid type can be
509 established. Dyke-hosted quartz veins are characterized by the occurrence of only type 4
510 fluids, but the dataset is weakly representative (n=3). Overall, the kinematics of the
511 structures hosting gold-bearing quartz appear to have a link with the established fluid
512 types. The implications of such a link are discussed below.

513

514 For the metamorphic facies of the host rocks (Supp. Table SM1, Fig. 9B), the quartz
515 samples in the greenschist facies are characterized by greater occurrences of type 1 fluids
516 (19%), but all other fluid types also occur. In the amphibolite facies, type 5 fluid is the
517 most abundant (14%), but all the other types are documented. For the hornfels facies,
518 represented only by the samples from Korup, fluids 1, 2, 4 and 5 are present. Overall,
519 although there are some variations from amphibolite to greenschist facies, no significant
520 relationship is detected between the metamorphic facies of the host rocks and the types of
521 fluids. The genetic implications are discussed below.

522

523 **9.4. Fluid type distribution**

524 The distribution of fluid types is of interest at the deposit and regional scales for defining
525 hydrothermal systems. Fluids of various types are commonly recorded at the deposit
526 scale. For example, the gold deposits of WG-03 (n=7) and Shereik-118 (n=5) record
527 various types of fluids (Fig. 10). However, Negeim records a unique and relatively
528 homogeneous fluid, a contrasting feature from other sites. It is noteworthy that type 1
529 fluid, the most complex in composition, occurs in all gold deposits with calculated
530 resources, such as UTM, Central (SCMC) and WG-03 (Fig. 10).

531

532 At the regional scale, the distribution of fluid types cannot be systematically linked with
533 the two established regional corridors (Fig. 4) or with the interpreted contour of the KSZ
534 (Fig. 1). Conversely, the spatial distribution of fluid types can be grouped within 3
535 discordant, NW-elongated fields (Fig. 10). The southern and northern fields are defined
536 by the occurrence of type 1 fluids. They are separated by a central field including Anas,
537 NW, SE, Negeim, Dardora and SE (Fig. 10), where fluids of types 1 and 3 are lacking.
538 However, fluids of type 2 are present for NW and Dardora. Fluids of type 4 are present at
539 Negeim. Fluids of type 5 are rather common, with samples at Dardora, NW and SE. This
540 central field thus appears to be dominated by fluids generated from a more localized
541 source. Except for the apparent NW-SE alignment of plutonic rocks in the northern field
542 (Fig. 10), there is no direct geological evidence supporting such an interpreted NW-
543 trending field. As orogenic gold deposits are related to deep processes (e.g., Gaboury,
544 2019; Groves et al., 2020), such apparent NW alignment may be related to deeper
545 inherited features and is discussed below.

546

547 **10. DISCUSSION**

548 The studied gold-bearing sites are distributed over a very large area and are associated
549 with two interpreted major regional deformation corridors and multiple intrusions.
550 Although restricted mostly to the quartz vein type, gold mineralization is hosted in
551 various metamorphic facies with different structural settings and specific hydrothermal
552 alterations. Furthermore, at least 6 types of fluids are documented. From a genetic

553 viewpoint, the main questions are as follows: 1) is gold mineralization related to single or
554 multiple events; 2) is there a more favourable structural setting for fluid upwelling and
555 forming economic gold deposits; 3) what are the fluid sources, and is there a better fluid
556 type for carrying gold; 4) what is the genetic significance of the various fluid types; 5)
557 what is the implication of the various metamorphic facies; and 6) what is the gold source?
558 These questions are addressed below.

559

560 **10.1. Single or multiple gold events**

561 All the studied gold-bearing sites and deposits exhibit mineralization that is structurally
562 controlled. For the vast majority of the mineralized sites, gold is hosted in S₂ high-strain
563 zones, cutting across the S₁ fabrics. These S₂ structures mostly strike NW to NE (Fig. 4),
564 corresponding to the last deformations recorded at the site scale. However, kinematic
565 regimes are different, ranging from reverse to reverse-oblique, normal, and strike-slip
566 with dextral and sinistral movements. At regional scale within KSZ (Fig. 4), the S₂ gold-
567 bearing fabric is correlative with the D₆ deformation of Abdelsalaman et al. (1998)
568 corresponding to local NE-trending dextral and NW-trending sinistral shear zones (Fig.
569 4). For the reverse and reverse-oblique S₂ gold-bearing shear zones, they can be formed
570 during the D₃ to D₅ shortening. However, they are most probably related to vertical
571 movement during the last D₆ transpressive deformation. It is also possible that gold
572 mineralization hosted in S₁ fabrics (Supp. Table SM1; Fig. 4) was introduced by
573 reactivation of pre-existing structures during D₆. The WG-03 is an example of such
574 reactivation as the mineralization within the S₁ and S₂ structures are the same (Supp.
575 Table SM1). Normal shear zones appear to be a late feature, probably post-dating the D₆
576 deformation.

577

578 Gold sites outside of the KSZ (Fig. 4: WG-03, Negeim, Sajid, Dardora, SE, and Korop)
579 share the same kinematics (strike-slip to reverse) and trending of their S₂ gold-hosting
580 fabrics with gold sites inside the KSZ. Genetically they are likely related to the regional
581 shortening corresponding to the D₆ deformation recorded in the KSZ. However, without
582 age of gold mineralization, it is impossible to establish if all sites are related to the same

583 mineralizing event. Nevertheless, most gold mineralizations are related to late structural
584 features consistent with the last deformations recorded by the KSZ.

585

586 **10.2. Implications of various structural settings**

587 Although major gold deposits can be hosted in various kinematic regimes (Gaboury,
588 2019), it is of interest to discuss the economic potential of the various structural settings.
589 The reverse shear veins show considerable thicknesses (> 3 m) and some depth continuity
590 (~ 400 m), despite the pinch and swell geometry that is typical of this type of mineralized
591 structure (e.g., Robert and Poulsen, 2001). In contrast, gold mineralization associated
592 with strike-slip movements forms very narrow but laterally quite continuous veins (> 1
593 km) occurring as a family of parallel veins, defining a mineralized area ~ 200 m wide.
594 However, the spacing between the individual veins (> 20 - 30 m) is large. Mineralization
595 in normal shear zones is, according to Supp. Table SM1, an unusual type regionally.
596 However, at the WG-03 deposit, numerous gold-bearing quartz veins are developed as
597 extensional features in previously mineralized shear zones from two different generations
598 (S_1 and S_2). Mineralization in these quartz veins may be the result of later gold
599 remobilization. Regionally, these extensional veins are late features and occur in zones
600 where other styles of mineralization are present (Fig. 4). They could then represent the
601 end of an important hydrothermal system active during crustal shortening up to the final
602 extensional exhumation (e.g., Wilkinson and Kesler, 2007). The mineralized dykes
603 appear to be the style with the greatest potential for ore volumes. In some cases, such as
604 Anas, mineralized dykes reach thicknesses > 20 m, with apparent continuities of several
605 tens of metres for the mineralization. Mineralization at Central C02 and C04 is also dyke-
606 hosted, and these dykes can be traced for tens of kilometres, although they do not
607 consistently contain gold.

608

609 An important element to highlight is the presence of different kinematic shear zones
610 hosting gold mineralization along the same trend. Three cases are noteworthy: the sectors
611 of Shereik, Anas-NW and Toubi (Fig. 4), which are all located along the West Corridor.
612 Moreover, the hydrothermal alterations are different according to the styles. These
613 variations can be explained by a major deformation zone having recorded gold

614 mineralizations at different times during its tectonic evolution. This aspect is developed
615 below on a regional scale.

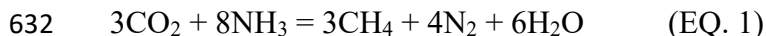
616

617 **10.3. Sources of volatiles in hydrothermal fluids**

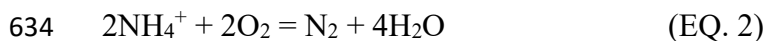
618 Our results reveal various assemblages of volatiles in fluid inclusions, such as 1)
619 aqueous-carbonaceous, 2) CO₂-rich, 3) H₂-bearing fluids, 4) C₂H₆-bearing fluids, 5) N₂-
620 CH₄-only fluids, and 6) water-only fluids. These were grouped into 6 types for genetic
621 considerations. It is also noteworthy that all analysed samples have fluid inclusions
622 containing nitrogen, except for the 2 samples with water-only fluids. The sources and
623 origins of these volatiles are discussed below to provide further constraints on the origin
624 of the fluids.

625

626 Sources of nitrogen have been discussed by Gaboury (2013). Three sources are possible
627 (Kreulen and Schuiling, 1982; Andersen et al., 1993). 1) Organic matter from sediments
628 may break down where nitrogen can be fixed in K-bearing silicates by substitution of K⁺
629 for NH₄⁺, notably in micas (e.g., Sadofsky and Bebout, 2000). 2) Hydrothermal alteration
630 of NH₄⁺-bearing silicates and formation of N₂ may occur by the equations postulated by
631 Kreulen and Schuiling (1982):



633 and by Wang et al. (2018) under oxidizing conditions between 350 and 600°C:



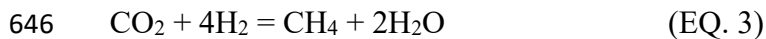
635 3) Primary N₂ may be liberated from magma or through metamorphism of the lower
636 crust. Consequently, nitrogen itself is not diagnostic for fluid sources.

637

638 N₂-CH₄-only fluids are quite atypical, documented only in some gold deposits, such as
639 the Maldon gold deposit in central Victoria, Australia (Fu et al., 2014). For this deposit,
640 CO₂-rich and N₂-CH₄-rich fluids coexist. Fu et al. (2014) proposed that genetically, N₂-
641 rich fluids were produced locally by NH₄-bearing phyllosilicate minerals in wall rock
642 slates (and/or by maturation of organic matter in shales) during contact metamorphism,
643 with limited involvement of high-temperature magmatic fluids.

644

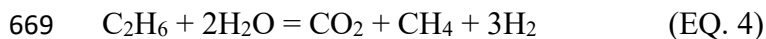
645 Methane alone can be generated by reduction following the reaction (Gaboury, 2013):



647 Metamorphic reactions involving carbonates with H₂ (Giardini and Salotti, 1969) and
648 serpentinization reactions (Abrajano et al., 1990; Huang et al., 2019; Reeves and Fiebig,
649 2020) can also produce CH₄.

650

651 In gold deposits, CO₂ can be sourced from the mantle and from metamorphic
652 devolatilization of volcanic-sedimentary rocks (e.g., Phillips and Powell, 1993;
653 Lowenstern, 2001; Lüders et al., 2015). In addition, CO₂-dominated fluids may be
654 sourced from felsic magmas (e.g., Kerrich, 1988; Connors et al., 1993; Xue et al., 2013).
655 Carbon dioxide-rich fluids have been documented in some orogenic gold deposits of
656 various ages (e.g., Gaboury, 2013). CO₂-rich and H₂O-poor fluid inclusions have been
657 reported from some important gold districts and deposits, such as Red Lake (Chi et al.,
658 2006), Ashanti (Mumm et al., 1997), Tarkwa goldfield (Klemd et al., 1997), Detour Gold
659 and Wona (Gaboury, 2013). In Sudan, such fluids have been recorded in the Hamadi gold
660 deposit (Cheng et al., 2017). The debate about the origin of CO₂-rich fluid inclusions
661 involves various possibilities (Klemd and Hirdes, 1997; Chi et al., 2006; Klein and
662 Fuzikawa, 2010; Hrstka et al., 2011), including 1) specific fluid sources from high-grade
663 metamorphism or early degassing of magmatic intrusions; 2) fluid-related processes such
664 as selective vapour accumulation following fluid immiscibility; two fluids operating
665 separately; or unmixing because of pressure fluctuations; and 3) post-entrapment
666 modifications of fluid inclusions. Recently, Gaboury (2013) proposed that CO₂-rich
667 fluids may be the result of the degradation of C₂H₆ and the consumption of H₂O, leading
668 to the progressive enrichment of CO₂ in the fluids, following the reaction:



670 In short, CO₂ can be generated from various sources, and there are numerous hypotheses
671 to account for CO₂-rich fluids in gold deposits.

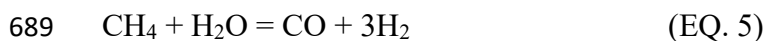
672

673 The sources and implications of C₂H₆ in fluids from orogenic gold deposits have been
674 documented by Gaboury (2013). It was demonstrated that C₂H₆ in hydrothermal fluids
675 cannot be produced from abiotic hydrothermal reactions involving CO₂ or CH₄ but rather

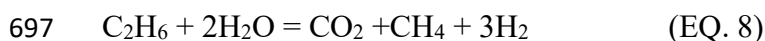
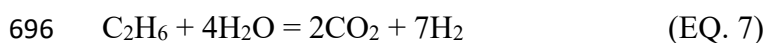
676 implies the interaction of fluids with thermally degraded organic matter. The record of
677 C₂H₆ in fluids from gold deposits confirms that organic matter-rich sedimentary rocks are
678 involved in the generation of fluids by metamorphism.

679

680 Hydrogen is not a common constituent of orogenic gold deposits (Gaboury, 2013), with
681 some exceptions (e.g., Ankusheva et al., 2019). The content of H₂ in fluid inclusions had
682 previously been considered doubtful, with the possibility of H₂ diffusion in mineral-
683 hosting fluid inclusions (e.g., Mavrogenes and Bodnar, 1994). Nevertheless, H₂ is not an
684 artefact of the analytical method because there is no H₂ production generated by
685 molecular fragmentation during ionization. Rather, hydrogen is a common product of
686 magmatic degassing at low pressure (e.g., Landis and Rye, 2005; Klein et al, 2020).
687 However, hydrothermal reactions in fluids, such as EQ. 4, can be proposed to account for
688 H₂. Methane can also produce H₂ following these reactions:



691 The reaction of EQ. 6 was experimentally tested and produced H₂ with catalysis from
692 315°C up to 700°C at atmospheric pressure (Guil-López et al., 2006). It is thus estimated
693 that with higher pressure and temperature corresponding to the amphibolite facies, this
694 reaction can produce H₂ from CH₄. According to Gaboury (2013), ethane can be
695 degraded in hydrothermal fluids by the following reactions to generate H₂:



698 Hydrothermal reactions involving the decomposition of light hydrocarbons can thus
699 account for the H₂ contents of the fluids.

700

701 **10.4. Sources of hydrothermal fluids**

702 For most gold deposits in metamorphic terranes, hydrothermal fluids can have
703 metamorphic or magmatic origins (e.g., Tomkins, 2013b; Goldfarb and Groves, 2015;
704 Gaboury, 2019) and even mixing of both (e.g., Augustin and Gaboury, 2019). Type 1
705 aqueous-carbonaceous fluid, with its very complex composition, including N₂, H₂, CH₄,
706 C₂H₆ and ±H₂, is most probably of metamorphic origin, generated by the metamorphism

707 of organic-rich sedimentary rocks to account for its signature with C₂H₆ (Gaboury, 2013;
708 Tomkins, 2013b). In addition, a carbonaceous metamorphic source, according to the
709 above review, accounts for the contents of N₂, H₂, and CH₄. Similar complex
710 metamorphic fluids have been documented for Detour Gold, the largest single Canadian
711 orogenic gold deposit, and for the Mana district, the most gold-endowed district in
712 Burkina Faso (Gaboury, 2013). Considering all the possible reactions above, type 1 fluid
713 is thus considered a primary, unmodified or weakly modified metamorphic fluid.

714

715 Type 2 fluid, similar to type 1 but with less water, certainly has an origin similar to that
716 of type 1 because it also contains C₂H₆. Nevertheless, its water content of less than 50%
717 is a strong indication that type 2 was generated by a different source than type 1.

718 Furthermore, as water-dominated fluid inclusions of group 1 are less abundant (Fig. 8E-
719 H), post-trapping modifications of fluid inclusions sourced from type 1 fluid can be ruled
720 out. A possible source is the metamorphism of sedimentary rocks richer in organic
721 material to account for the higher proportion of carbon-bearing volatiles.

722

723 Type 3 fluid, similar to type 1 but without C₂H₆, probably has the same source, where
724 C₂H₆ could have been consumed by hydrothermal reactions (EQs. 7 and 8: Gaboury,
725 2013), or it may be sourced from the metamorphism of sedimentary rocks less rich in
726 organic matter or from volcanic rocks. The former hypothesis appears more valid as type
727 3 fluid systematically coexists with type 1 in WG-03, WG-14, Yasmine, Toubi, Shereik-
728 118 and Korup (Supp. Table SM3; Fig. 10).

729

730 Type 4 fluids are aqueous-carbonaceous fluids with nitrogen but are devoid of
731 hydrocarbons. Genetically, they can be sourced from 1) intrusions, 2) metamorphic
732 devolatilization, and 3) phase separation from a more complex parental fluid. Phase
733 separations between liquid- and vapour-rich phases are induced by pressure drops (e.g.,
734 Robert et al., 1995; Wilkinson, 2001). The coexistence of liquid- and vapour-rich fluid
735 inclusions is considered as evidence that fluid modification occurred by the physical
736 process of phase separations. The phase separation hypothesis likely occurred at sites
737 where fluids of types 1 or 3 coexist with type 4 fluid, such as Korup, WG-03, Shereik-

738 118, and Yasmine. For Negeim, because the 3 samples have very similar compositions,
739 phase separation is not supported by the data. Consequently, a specific fluid from a
740 magmatic source cannot be ruled out. Other sites having only type 4 are Anas and SW-1
741 with only one sample.

742

743 Type 5 fluids are water-devoid fluids with various combinations of CO₂, N₂, and CH₄
744 volatiles, including specific fluids such as CO₂-only and N₂-CH₄ fluids. The origin of
745 these fluids could be diverse, as reviewed above. However, phase separation appears to
746 be the preponderant mechanism to account for these fluids, especially at sites where
747 fluids of type 1 or 3 coexist with type 5 fluid, such as Korup, WG-03 and Shereik. Phase
748 separation is also supported by the petrographic characteristics of fluid inclusions: the
749 samples with type 5 fluids only have gaseous fluid inclusions of groups 2 and 3.

750 Specifically, samples from SE, with fluids of types 5 and 6 (water-only), could be prime
751 examples of this extreme phase separation. Nevertheless, such fluids at SE, Dardora and
752 NW could have a different origin, such as magmatic, even if phase separation was an
753 efficient mechanism. Finally, type 6 fluids with only water, occurring at SE and Shereik,
754 can also be related to phase separation.

755

756 Fluids of types 1 and 2, which are C₂H₆-bearing, were generated by the deeper
757 metamorphism of organic-rich matter from sedimentary rocks, such as black shales.
758 These rocks have also been proposed as the principal gold source for orogenic gold
759 deposits (e.g., Large et al., 2011; Tomkins, 2010; Tomkins, 2013b; Gaboury, 2013;
760 2019). Pyritic black shales have been intersected in the drill holes (Fig. SM2E-F) of the
761 Central deposit (SCMC). Consequently, such favourable rocks occur in the study area,
762 especially within the sedimentary rocks of the KSZ. These fluids are therefore considered
763 the most important for generating significant orogenic gold deposits.

764

765 Different fluid types can be interpreted as the manifestation of different hydrothermal
766 systems. We propose that the various types of fluids were generated from a primary fluid
767 (types 1 and 2) that evolved by hydrothermal reactions and/or phase separations to
768 generate types 3 to 6. Nevertheless, the possibility of numerous specific hydrothermal

769 systems cannot be eliminated (see below). Our interpretation is supported by the fluid
770 inclusion groups (Fig. 8), the occurrence of various types of fluids in the same deposits
771 (Fig. 10), and the relative abundance and wide distribution of types 1 and 2 fluids in the
772 study area (Supp. Table SM3. Figs. 7 and 10).

773

774 **10.5. Hydrothermal systems**

775 Metamorphic devolatilization for generating fluids is a regional process that can form
776 large fields of gold mineralization extending tens of kilometres (Phillips and Powell,
777 2010). Although more than 6 types of fluid signatures are established in the study area,
778 all can be generated by phase separations or hydrothermal reactions from a primary fluid
779 having the complex composition of fluid type 1 or type 2. Consequently, it is
780 questionable to distinguish different hydrothermal systems based only on the fluid types.
781 Furthermore, a single vein or even a group of veins forming a deposit can have recorded
782 various fluid signatures (Gaboury, 2013).

783

784 Nevertheless, specific hydrothermal systems can be interpreted by combining fluid types,
785 structural settings and the spatial distribution of gold mineralization. In the northern part,
786 a single hydrothermal system can be identified at WG-03, UTM, Central and WG-14.
787 Specifically, they share fluid of type 1 with reverse settings of gold mineralization,
788 although later extensional gold-bearing quartz veins occur at WG-03 (Figs. 4 and 10).
789 Toubi, with its reverse-oblique setting and type 1 fluid, can also be included in this large
790 hydrothermal system.

791

792 Other systems are not so simple to separate and are probably superposed systems. For
793 example, along the West Corridor, Toubi, Anas, NW and Shereik share gold
794 mineralization hosted in various structural settings and variable metamorphic facies with
795 all 6 types of fluids. In addition, they are distributed along a >250 km-long corridor.
796 Numerous hydrothermal systems are thus expected, rather than one that evolved to
797 produce all types of fluids. Such an interpretation of multiple systems is also recorded at
798 the deposit scale. At Shereik (Figs. 4 and 10), there is a diversity of structural settings and
799 fluids, which is more consistent with superposed hydrothermal systems.

800

801 Along the East Corridor and in the eastern part, Yasmine, SW, Negeim, Dardora and SE
802 are located around an interpreted large central pluton (Fig. 2). They have various settings,
803 from dextral to reverse and sinistral (Fig. 4) and various types of fluids (Fig. 10).

804 Nevertheless, no adjacent site shares structural setting and fluids with another (Figs. 4
805 and 10). They are thus interpreted as formed from separate and specific hydrothermal
806 systems. This interpretation is supported by the Negeim deposit, where fluids are only of
807 type 4 with a possible magmatic origin.

808

809 In the southern part, the gold at Sajid and Korup is hosted in sinistral and dextral settings,
810 respectively. Both sites record type 1 and type 2 fluids. They can be the result of a single
811 hydrothermal system but with different strike-slip movements. Furthermore, they are
812 located away from the KSZ but along the projection of the Nakasib suture zone (Fig. 1).

813

814 These interpretations, combining structural settings and fluid types, imply numerous
815 hydrothermal systems. Such an interpretation is consistent with the actual knowledge of
816 gold-endowed major faults, such as the Cadillac-Lader Lake fault in Canada (Bedeaux et
817 al., 2017; In press), where specific segments recorded different hydrothermal systems at
818 different times.

819

820 **10.6. Implications of the metamorphic facies**

821 Most orogenic gold deposits are hosted in greenschist-facies rocks, where metamorphic
822 fluids are generated below the greenschist-amphibolite transition (Tomkins, 2010; Finch
823 and Tomkins, 2017; Gaboury, 2019). Our data indicate that some important deposits,
824 such as WG-03 and Shereik (Fig. 4), record the various types of fluids (Fig. 10) and
825 retrograde hydrothermal alteration even hosted in rocks in the amphibolite facies (Supp.
826 Table SM1). Such an atypical context can be explained by diachronic metamorphism:
827 early amphibolite-facies metamorphism of the host rocks and later metamorphism of the
828 underlying sedimentary rocks to generate retrograde mineralizing fluids. Such a model
829 implies obduction or nappe transport of metamorphosed rocks over non-metamorphosed
830 sedimentary rocks. The KSZ, which is a collisional belt, can provide such a tectonic

831 accretionary context. For example, it is possible that metamorphosed rocks at WG-03
832 were thrust over sedimentary rocks during the closure of the sedimentary basin now
833 manifested by the KSZ. According to Abdelsalam (1995), the E-W, shallowly north-
834 dipping S_1 fabric is related to the development of D_1 S-verging folds associated with
835 ophiolitic nappe emplacement during the closure of the Atmur-Delgo oceanic suture.

836

837 For Shereik, this area is interpreted as an exotic nappe (Fig. 1; Evuk et al., 2014). The
838 penetrative shallowly dipping S_1 foliation (Fig. 5E) more evident at Shereik than at the
839 other study sites, and the stretching lineations indicate a thrusting movement towards the
840 NE. Nevertheless, the mineralization is retrograde, with strong iron carbonate alteration
841 (Fig. 5E) and quartz veining.

842

843 In short, the closure of the sedimentary basin, now represented by the KSZ, is considered
844 to have provided fluid-bearing rocks underneath already cratonized rocks or
845 metamorphosed nappes to generate retrograde mineralizing metamorphic fluids.

846 Consequently, gold mineralization can occur away from the interpreted limit of the KSZ,
847 as suggested by the location of the WG-03 deposit.

848

849 **10.7. Sources of gold**

850 The sources of gold for orogenic deposits have been reviewed by numerous authors (e.g.,
851 Pitcairn et al., 2010; Large et al., 2011; Tomkins, 2013b; Goldfarb and Groves, 2015;
852 Pitcairn et al.; 2015; Gaboury, 2019). Organic-rich and pyritic sedimentary rocks are
853 considered one of the most important sources. Gold and other trace metals originally
854 hosted in sedimentary pyrite can be liberated by recrystallization and hydrothermal
855 replacement processes at metamorphic temperatures corresponding to the pyrite–
856 pyrrhotite transition (Pitcairn et al., 2010; Large et al., 2011; Zhong et al., 2015; Finch
857 and Tomkins, 2017; Wu et al., 2020). Gaboury (2019) concludes that the fluids, ligands,
858 and gold are all sourced from the metamorphism of the same carbonaceous and pyrite-
859 rich sedimentary rocks. Such deep processes are recorded in mineralizing fluids by the
860 presence of ethane (Gaboury, 2013). For the northern part of the Nubian Shield, Abu-
861 Alam et al. (2018) also reached the same conclusion that gold-bearing fluids were

862 generated by metamorphic devolatilization at the greenschist–amphibolite facies
863 transition of the ophiolite and sedimentary rocks.

864

865 A link between gold dissolved in oceans and the temporal distribution of orogenic gold
866 deposits was first proposed by Tomkins (2013a) and documented by Large et al. (2015)
867 using gold concentrations in primary pyrites from black shales. Oxidizing seawater
868 conditions were favourable for fixing gold in nodular sedimentary pyrite, accounting for
869 the gold endowment in black shales (Large et al., 2015). The lack of major orogenic gold
870 deposits from 1800 to 800 Ma is explained by the low levels of Au in the oceans during
871 this period (Large et al., 2015), which corresponds to the Canfield Ocean (Canfield,
872 1998). During the middle to late Proterozoic, the deep oceans were anoxic and sulfidic
873 (Canfield, 1998), hence limiting the bacterial reduction of sulfate and the incorporation of
874 gold in nodular pyrite (Gaboury, 2019). The occurrence of orogenic gold deposits in
875 Neoproterozoic time, such as those along the KSZ in Sudan, coincides with the
876 reappearance of oxygenic conditions in the oceans (Large et al., 2015; Steadman et al.,
877 2020). Ethane in fluids related to gold mineralization is thus an indication that gold was
878 sourced from the metamorphism of favourable organic-rich and gold-bearing pyritic
879 sedimentary rocks.

880

881 **10.8. Geodynamic evolution and gold deposit formation**

882 A geodynamic model for the formation of the KSF was proposed by Evuk (2013). The
883 model involves the formation of an oceanic basin from 900 to 850 Ma (Fig. 11A). Later,
884 from 850 to 630 Ma, double subduction is interpreted to accommodate the convergent
885 tectonic regime (Fig. 11B). We proposed that during this period, organic-rich shales
886 accumulated under oceanic conditions favourable for gold incorporation within primary
887 pyrite. At the end, limestone precipitated at the top of the stratigraphic succession.
888 Finally, during the collisional stage, between 630 and 500 Ma, the volcanic-sedimentary
889 rocks of the Keraf suture basin were folded, thrust faulted and metamorphosed.
890 Metamorphic gold-bearing fluids were generated by the rebound of the metamorphic
891 isograds (Fig. 11C). Gold deposits were formed in the KSZ and locally in the cratons
892 adjacent to the suture zone. The studied gold occurrences are considered orogenic

893 because they share the same characteristics in terms of structural settings, styles and
894 hydrothermal alterations as classic orogenic gold deposits.

895

896 **11. CONCLUSION**

897 The study areas show diverse structural settings for orogenic gold mineralization hosted
898 in greenschist- and amphibolite-facies rocks. Most gold mineralizations occur in late S₂
899 shear zones correlated with the regional D₆ deformation of Abdelsalam et al. (1998).

900 Reverse movements and dyke host rocks are considered the most favourable settings for
901 forming gold deposits with economic potential. Two major corridors of deformation are
902 delineated, but only the West Corridor seems to play a real role in the mineralization,
903 based on the number of gold sites and their dominant reverse structural regime.

904

905 Six types of hydrothermal fluids are distinguished based on specific volatile contents and
906 proportions. Most of them can be related to fluid evolution by hydrothermal reactions
907 and/or phase separations from a primitive fluid of metamorphic origin. Hydrothermal
908 fields are identified based on structural settings and fluid types. The northern field is
909 interpreted as a single large hydrothermal system accounting for the mineralization at the
910 WG-03, UTM and Central deposits as well as WG-14 and possibly Toubi sites. For sites
911 along the West Corridor, such as Toubi, Anas, NW and Shereik, multiple and
912 overlapping hydrothermal systems are proposed to explain the various fluid types and
913 structural settings. Conversely, other sites, such as SW, Yasmine, Korup, Saijd, Dardora,
914 Negeim, and SE, appear to have been formed by more localized individual hydrothermal
915 systems, even with a possible magmatic contribution to Negeim.

916

917 The most important outcome of this study is the documentation of fluids containing
918 ethane at numerous sites and deposits. Ethane is an indication that fluids were generated
919 by the metamorphism of carbonaceous-pyritic sedimentary rocks (Gaboury, 2013). These
920 rocks are also considered one of the best sources for providing ligands and gold for the
921 formation of orogenic gold deposits (Gaboury, 2019). The KSZ, which is composed
922 mainly of turbidites, provided such source rocks deeper in the suture zone and below the
923 adjacent cratons during the collision. The studied orogenic gold sites and deposits in

924 various structural contexts and metamorphic facies are thus attributed to the deeper
925 metamorphism of these favourable rocks.

926

927 Finally, this study adds support to a general model for the formation of orogenic gold
928 deposits from Archaean to Palaeozoic time (Gaboury, 2013, Gaboury, 2019), involving
929 gold extraction by metamorphism of primary pyrite in organic-rich sediments, as far as
930 oceanic conditions were favourable for gold enrichment in pyrite (Large et al., 2015;
931 Steadman et al., 2020).

932

933 **Acknowledgements**

934

935 This paper is based on fieldwork by the first author supported by MANAGEM and its
936 Sudanese subsidiary Manub. Numerous geologists were involved during fieldwork, and
937 they are thanked for sharing their knowledge. In particular, Mourad Iliani and Moujahid
938 Min Allah assisted D. Gaboury in the field, and without them, this contribution would
939 have been impossible. We are grateful to Prof. S.A.S. Dare (UQAC) for proofreading.
940 The manuscript was substantially improved by comments from M. Leybourne, J.
941 Steadman and anonymous reviewers.

942

943 **REFERENCES**

- 944 Abdelsalam, M.G., Stern, R.J., 1996a, Mapping Precambrian structures in the Sahara
945 Desert with SIR641 C/X-SAR radar: The Neoproterozoic Keraf Suture, NE Sudan:
946 *Journal of Geophysical Research: Planets*, v. 101, p. 23063–23076.
947 <https://doi.org/10.1029/96JE01391> 643
- 948 Abdelsalam, M.G., and Stern, R.J., 1996b, Sutures and shear zones in the Arabian-
949 Nubian Shield: *Journal of African Earth Sciences*, v. 23, p. 289–310.
950 [https://doi.org/10.1016/S0899-5362\(97\)00003-1](https://doi.org/10.1016/S0899-5362(97)00003-1) 645
- 951 Abdelsalam, M.G., Stern, R.J., Schandelmeier, H., Sultan, and M., 1995, Deformational
952 History of the Neoproterozoic Keraf Zone in NE Sudan, Revealed by Shuttle
953 Imaging Radar: *The Journal of Geology*, v. 103, p. 475–491.
954 <https://doi.org/10.1086/629771>

955 Abdelsalam, M.G., Stern, R.J., Copeland, P., Elfaki, E.M., Elhur, B., and Ibrahim, F.M.,
956 1998, The Neoproterozoic Kerf Suture in Ne Sudan: Sinistral Transpression Along
957 the Eastern Margin of West Gondwana: *The Journal of Geology*, v. 106, p. 133–
958 148. <https://doi.org/10.1086/516012> 648

959 Abdelsalam, M.G., Liégeois, J.-P., and Stern, R.J., 2002, The Saharan Metacraton:
960 *Journal of African Earth Sciences*, v. 34, p. 119–136.

961 Abdelsalam, M.G., Abdel-Rahman, E.-S.M., El-Faki, E.-F.M., Al-Hur, B., El-Bashier, F.-
962 R.M., Stern, R.J., and Thurmond, A.K., 2003, Neoproterozoic deformation in the
963 northeastern part of the Saharan Metacraton, northern Sudan: *Precambrian Research*,
964 v. 123, p. 203–221.

965 Abrajano, T.A., Sturchio, N.C., Kennedy, B.M., Lyon, G.L., Muehlenbachs, K., and
966 Bohlke, J.K., 1990, Geochemistry of reduced gas related to serpentinization of the
967 Zambales ophiolites, Philippines: *Applied Geochemistry*, v. 5, p. 625–630.
968 doi:10.1016/0883-2927(90)90060-I

969 Adam, M.M.A., Lv, X., Rahman, A.A.A., Stern, R.J., Abdalrhman, A.A.A., and Ullah,
970 Z., 2020, In-situ sulfur isotope and trace element compositions of pyrite from the
971 Neoproterozoic Haweit gold deposit, NE Sudan: Implications for the origin and
972 source of the sulfur: *Ore Geology Reviews*, v. 120, 103405.
973 doi.org/10.1016/j.oregeorev.2020.103405

974 Abu-Alam, T., El Monsef, M.A., and Grosch, E. 2018, Shear-zone hosted gold
975 mineralization of the Arabian– Nubian Shield: devolatilization processes across the
976 greenschist–amphibolite-facies transition, *In Ferrero, S., Lanari, P., Goncalves, P.,*
977 *Grosch, E.G., eds., Metamorphic Geology: Microscale to Mountain Belts:*
978 *Geological Society, London, Special Publications*, v. 478, p. 287-313.
979 doi.org/10.1144/SP478.13

980 Almond, D.C., and Ahmed, F., 1987, Ductile shear zones in the northern Red Sea Hills of
981 Sudan and their implications for crustal collision. *Geological Journal*, v. 22, p. 175-
982 184.

983 Almond, D.C., Ahmed, F., and Shaddad, M.Z., 1984, Setting of gold mineralization in
984 the northern Red Sea Hills of Sudan: *Economic Geology*, v. 79, p. 389–392.
985 doi:10.2113/gsecongeo.79.2.389

986 Andersen, T., Austrheim, H., Burke, E.A.J., and Elvevold, S., 1993, N₂ and CO₂ in deep
987 crustal fluids: Evidence from the Caledonides of Norway: *Chemical Geology*, v.
988 108, p. 113–132. doi:10.1016/0009-2541(93)90320-I.

989 Ankusheva, N.N., Palenova E.E., and Shanina, S.N., 2019, Fluid Inclusion Evidences for
990 the P-T Conditions of Quartz Veins Formation in the Black Shale-Hosted Gold
991 Deposits, Bodaybo Ore Region, Russia: *Journal of Earth Science*,
992 <https://doi.org/10.1007/s12583-019-1024-5>.

993 Augustin, J., and Gaboury, D., 2019, Multi-stage and multi-sourced fluid and gold in the
994 formation of orogenic gold deposits in the world-class Mana district of Burkina
995 Faso - Revealed by LA-ICP-MS analysis of pyrites and arsenopyrites. *Ore Geology*
996 *Review*, v. 104, p. 495–521.

997 Bailo, T., 2000, Keraf shear zone, NE Sudan: geodynamic characteristics of the Nile
998 craton-Nubian Shield boundary. Ph.D. Thesis. Geowissenschaften der Technischen
999 Universität Berlin, 141 p.

1000 Bailo, T., Schandelmeier, H., Franz, G., Sun, C.H., and Stern, R.J., 2003, Plutonic and
1001 metamorphic rocks from the Keraf Suture (NE Sudan): A glimpse of
1002 Neoproterozoic tectonic evolution on the NE margin of W. Gondwana:
1003 *Precambrian Research*, v. 123, p. 67–80. doi:10.1016/S0301-9268(03)00044-5.

1004 Barrie, C.T., Abdalla, M.A.F., R. and Hamer, D., 2016, Volcanogenic Massive Sulphide–
1005 Oxide Gold Deposits of the Nubian Shield in Northeast Africa: *In* Bouabdellah, M.,
1006 and Slack, J., eds., *Mineral Deposits of North Africa*, Mineral Resource Reviews:
1007 Springer, Cham, p. 417-435. DOI 10.1007/978-3-319-31733-5_17

1008 Bedeaux, P., Pilote, P., Daigneault, R., and Rafini, S., 2017, Synthesis of the structural
1009 evolution and associated gold mineralization of the Cadillac Fault, Abitibi, Canada:
1010 *Ore Geology Reviews*, v. 82, p. 49-69.

1011 Bedeaux, P., Brochu, A., Mathieu, L., Gaboury, D., and Daigneault, R., In Press,
1012 Structural analysis and metamorphism of the Barlow Fault Zone, Chibougamau
1013 area, Neoproterozoic Abitibi Subprovince: implications for gold mineralization.
1014 *Canadian Journal of Earth Sciences*.

- 1015 Bertrand, J.-M., and Caby, R., 1978, Geodynamic evolution of the PanAfrican orogenic
1016 belt: A new interpretation of the Hoggar Shield (Algerian Sahara): *Geologische*
1017 *Rundschau* v. 67, p. 357–388.
- 1018 Black, R., and Liégeois, J.P., 1993, Cratons, mobile belts, alkaline rocks and continental
1019 lithospheric mantle: The Pan-African testimony: *Journal of the Geological Society*,
1020 v. 150, p. 89–98.
- 1021 Boullier, A.-M., and Robert, F., 1992, Palaeoseismic events recorded in Archaean gold-
1022 quartz vein networks, Val d'Or, Abitibi, Quebec, Canada: *Journal of Structural*
1023 *Geology*, v. 14, p. 161-179.
- 1024 Botros, N.S., 2002, Metallogeny of gold in relation to the evolution of the Nubian Shield
1025 in Egypt: *Ore Geology Reviews*, v. 19, p. 137–164.
- 1026 Botros, N.S., 2004, A new classification of the gold deposits of Egypt, *Ore Geology*
1027 *Reviews*, v. 25, p. 1-37.
- 1028 Canfield, D., 1998, A new model for Proterozoic ocean chemistry: *Nature*, v. 396, p.
1029 450–453. <https://doi.org/10.1038/24839>
- 1030 Cheng, X.H., Xu, J.H., Wang, J.X., Xue, Q.P., and Zhang, H., 2017, Carbonic fluids in
1031 the Hamadi gold deposit, Sudan: origin and contribution to gold mineralization:
1032 *Canadian Journal of Earth Sciences*, v. 54, p. 494–511.
- 1033 Chi, G.X., Dubé, B., Williamson, K., and Williams-Jones, A.E., 2006, Formation of the
1034 Campbell-Red Lake gold deposit by H₂O-poor, CO₂-dominated fluids: *Mineralium*
1035 *Deposita*, v. 40, p. 726–741. doi:10.1007/s00126-005-0029-3.
- 1036 Connors, K.A., Noble, D.C., Bussey, S.D., and Weiss, S.I., 1993, Initial gold contents of
1037 silicic volcanic rocks: bearing on the behavior of gold in magmatic systems:
1038 *Geology*, v. 21, p. 937–940.
- 1039 Dusel-Bacon, C. 2012, Petrology of metamorphic rocks associated with volcanogenic
1040 massive sulfide deposits. In Shanks III, W.C. P. and Thurston, R., eds.,
1041 *Volcanogenic massive sulfide occurrence model*. U.S. Geological Survey Scientific
1042 *Investigations Report 2010–5070 –C*, chap. 17, p. 277-288.
- 1043 El Aref, M., El-Rahman, Y. A., Zoheir, B., Surour A., Helmy, H.M, Abdelnasser A.,
1044 Ahmed, A.H., and El-Ahmadi Ibrahim, M., 2020, Mineral Resources in Egypt (I):
1045 *Metallic Ores*. In Hamimi, Z., El-Barkooky, A., Martínez Frías, J., Fritz, H., and

1046 Abd El-Rahman, Y., eds., The Geology of Egypt. Regional Geology Reviews.
 1047 Springer, Cham, p. 521-587. doi.org/10.1007/978-3-030-15265-9_14

1048 El-Gaby, S., List, F.K., and Tehrani, R., 1988, Geology, evolution and metallogenesis of
 1049 the Pan African Belt in Egypt. *In* El-Gaby, S., and Greiling, R.O., Eds., The Pan
 1050 African Belt of Northeast Africa and Adjacent Areas. Vieweg, Braunschweig, p.
 1051 17–63.

1052 Evuk, D., 2013. Geodynamic evolution of the central-eastern Bayuda Desert Basement,
 1053 Sudan: Structural, petrological, geochemical and geochronological investigations.
 1054 Unpublished PhD thesis. Technical University of Berlin. 193 p.

1055 Evuk, D., Franz, G., Frei, D., and Lucassen, F., 2014, The Neoproterozoic evolution of
 1056 the central-eastern Bayuda Desert (Sudan): *Precambrian Research*, v. 240, p. 108–
 1057 125.

1058 Finch, E.G., and Tomkins, A.G., 2017, Pyrite-pyrrhotite stability in a metamorphic
 1059 aureole: implications for orogenic gold genesis: *Economic Geology*, v. 112, p. 661–
 1060 674.

1061 Fritz, H., Abdelsalam, M., Ali, K.A., Bingen, B., Collins, A., Fowler, A.R., Ghebreab,
 1062 W., Hauzenberger, C.A., Johnson, P.R., Kusky, T.M., Macey, P., Muhongo, S.,
 1063 Stern, R.J., and Viola, V., 2013, Orogen styles in the East African Orogen: a review
 1064 of the Neoproterozoic to Cambrian tectonic evolution: *Journal of African Earth
 1065 Sciences*, v. 86, p. 65-106.

1066 Fu, B., Mernagh, T.P., Fairmaid, A.M., Phillips, D., and Kendrick, M.A., 2014, CH₄-N₂
 1067 in the Maldon gold deposit, central Victoria, Australia: *Ore Geology Reviews*, v.
 1068 58, p. 225–237. doi:10.1016/j.oregeorev.2013.11.006.

1069 Gaboury, D., 2013, Does gold in orogenic deposits come from pyrite in deeply buried
 1070 carbon-rich sediments?: Insight from volatiles in fluid inclusions: *Geology* v.
 1071 41, p. 1207–1210. doi.org/10.1130/G34788.1

1072 Gaboury, D., 2014, Rapport de visite géologique projet Gabgaba, Soudan.
 1073 Unpublished report to MANAGEM, April 29th, 20 p.

1074 Gaboury, D., 2015, Geometrical characteristics and origin of the gold mineralisation
 1075 at the WG-03 deposit, Gabgaba Project, Sudan. Unpublished report to Manum,
 1076 June 14th, 54 p.

1077 Gaboury, D., 2019, Parameters for the formation of orogenic gold deposits: Applied
1078 Earth Science, v. 128, p. 124-133, DOI: 10.1080/25726838.2019.1583310

1079 Gaboury, D., Keita, M., Guha, J., and Lu, H.-Z., 2008, Mass spectrometric analysis of
1080 volatiles in fluid inclusions decrepitated by controlled heating under vacuum.
1081 Economic Geology, v. 103, p. 439–443.

1082 Garofalo, P.S., Fricker, P.S., Gunther, M.B., Bersani, D., Lotticci, P.P., 2014.
1083 Physical–chemical properties and metal budget of gold-transporting
1084 hydrothermal fluids in orogenic deposits. In: Garofalo, P.S., Ridley, J.R. (Eds.),
1085 Gold-transporting Hydrothermal Fluids in the Earth's Crust. Geological Society
1086 Special Publication 402, pp. 71–102.

1087 Ghebreab, W., Greiling, R.O., and Solomon, S., 2009, Structural setting of
1088 Neoproterozoic mineralization, Asmara district, Eritrea: Journal of African Earth
1089 Sciences, v. 55, p. 219-235.

1090 Giardini, A.A., and Salotti, C.A., 1969, Kinetics and relations in the calcite-hydrogen
1091 reaction and reactions in the dolomite-hydrogen and siderite-hydrogen systems:
1092 The American Mineralogist, v. 54, p. 1151–1172.

1093 Goldfarb, R.J., and Groves, D.I., 2015. Orogenic gold: common vs evolving fluid and
1094 metal sources through time: Lithos, v. 223, p.2–26.

1095 Goldfarb, R.J., Bradley, D., and Leach, D.L., 2010. Secular variation in economic
1096 geology. Economic Geology, v. 105, p. 459–465.
1097 doi:10.2113/gsecongeo.105.3.459.

1098 Greenwood, W.R., Anderson, R.E., Fleck, R.J., and Roberts, R.J., 1980, Precambrian
1099 geologic history and plate tectonic evolution of the Arabian Shield: Saudi Arabia
1100 Directorate General Mineral Resources Bulletin, v. 24, p. 24–35.

1101 Guha, J., Lu, H., and Gagnon, M., 1990, Gas composition of fluid inclusions using
1102 solid probe mass spectrometry and its application to study of mineralizing
1103 processes. Geochimica et Cosmochimica Acta, v. 54, 553–558.

1104 Guil-López, R., La Parola, V., Pena, M.A., and Fierro, J.L.G., 2006, Hydrogen
1105 production via CH₄ pyrolysis: Regeneration of ex hydrotalcite oxide catalysts:
1106 Catalysis Today, v. 116, p. 289–297.

1107 Groves, D.I., Santosh, M., Deng, J., Wang, Q., Yang L., and Zhang L., 2020. A
1108 holistic model for the origin of orogenic gold deposits and its implications for
1109 exploration: *Mineralium Deposita*, v. 55, p. 275–292.

1110 Harms, U., Darbyshire, D.P.F., Denkler, T., Hengst, M., and Schandelmeier, H., 1994.
1111 Evolution of the Neoproterozoic Delgo suture zone and crustal growth in
1112 northern Sudan: geochemical and radiogenic isotope constraints: *Geologische*
1113 *Rundschau*, v. 83, p. 591–603.

1114 Helmy, H.M., Kaindl, R., Fritz, H., and Loizenbauer, J., 2004, The Sukari gold mine,
1115 Eastern Desert, Egypt: structural setting, mineralogy and fluid inclusion study:
1116 *Mineralium Deposita*, v. 39, p. 495–511.

1117

1118 Hrstka, T., Dubessy, J., and Zachariáš, J., 2011, Bicarbonate-rich fluid inclusions and
1119 hydrogen diffusion in quartz from the Libčice orogenic gold deposit, Bohemian
1120 Massif: *Chemical Geology*, v. 281, p. 317–332, doi:10.1016/j.chemgeo.2010
1121 .12.018.

1122 Huang, R., Sun, W., Song, M., and Ding, X., 2019, Influence of pH on Molecular
1123 Hydrogen (H₂) Generation and Reaction Rates during Serpentinization of Peridotite
1124 and Olivine: *Minerals*, v. 9, 661. <https://doi.org/10.3390/min9110661>

1125 Jamasmie, C., 2020, Endeavour Mining walks away from a takeover talk with
1126 Centamin: *The Northern Miner*, v. 6 (2), p. 3.

1127 Johnson, P.R., and Woldehaimanot, B., 2003, Development of the Arabian-Nubian
1128 Shield; perspectives on accretion and deformation in the northern East African
1129 Orogen and the assembly of Gondwana: Geological Society, London, Special
1130 Publications, v. 206, p. 289–325.

1131 Johnson, P.R., Andresen, A., Collins, A.S., Fowler, A.R., Fritz, H., Ghebreab, W., Kusky,
1132 T.M., and Stern, R.J., 2011, Late Cryogenian–Ediacaran history of the Arabian–
1133 Nubian Shield: A review of depositional, plutonic, structural, and tectonic events in
1134 the closing stages of the northern East African Orogen: *Journal of African Earth*
1135 *Sciences*, v. 61, p. 167–232.

1136 Johnson, P.R., Zoheir, B.A., Ghebreab, W., Stern, R.J., Barrie, C.T., and Hamer, R.D.,
1137 2017, Gold-bearing volcanogenic massive sulfides and orogenic-gold deposits in
1138 the Nubian Shield: *South African Journal of Geology*, v. 120, p. 63-76.

1139 Karmakar, S., and Schenk, V., 2015, Neoproterozoic metamorphic events along the
1140 eastern margin of the East Sahara Ghost Craton at Sabaloka and Bayuda, Sudan:
1141 Petrology and texturally controlled in-situ monazite dating: *Precambrian Research*,
1142 v. 269, p. 217–241.

1143 Kerrich, R., 1976, Some effects of tectonic recrystallization on fluid inclusions in vein
1144 quartz: *Contributions to Mineralogy and Petrology*, v. 59, p. 195–202.

1145 Kerrich, R., 1988, Archean gold: Relation to granulite formation or felsic intrusions?:
1146 *Geology*, v. 17, p. 1011–1015.

1147 Klein, E.L., and Fuzikawa, K., 2010, Origin of the CO₂-only fluid inclusions in the
1148 Palaeoproterozoic Carará vein-quartz gold deposit, Ipitinga Auriferous District, SE
1149 Guiana Shield, Brazil: Implications for orogenic gold mineralisation: *Ore Geology
1150 Reviews*, v. 37, p. 31–40. doi:10.1016/j.oregeorev.2009.10.001.

1151 Klein, F., Tarnas, J.D., and Bach, W., 2020, Abiotic Sources of Molecular Hydrogen on
1152 Earth: *Elements*, v. 16, p. 19–24. doi.org/10.2138/gselements.16.1.19

1153 Klemd, R., and Hirdes, W., 1997, Origin of an unusual fluid composition in Early
1154 Proterozoic Palaeoplacer and lode-gold deposits in Birimian greenstone terranes of
1155 West Africa: *South African Journal of Geology*, v. 100, p. 405–414.

1156 Klemm, R., and Klemm, D., 2013, Gold and Gold Mining in Ancient Egypt and Nubia:
1157 *Natural Science in Archaeology*, v. 341. DOI 10.1007/978-3-642-22508-6_6,
1158 Springer-Verlag, Berlin and Heidelberg.

1159 Klemm, D., Klemm, R., and Murr, A., 2001, Gold of the Pharaohs – 6000 years of
1160 gold mining in Egypt and Nubia: *Journal of African Earth Sciences*, v. 33, p.
1161 643-659.

1162 Kreulen, R., and Schuiling, R.D., 1982, N₂–CH₄–CO₂ fluids during formation of the
1163 Dôme de l'Agout, France: *Geochimica et Cosmochimica Acta*, v. 46, p. 193–203.
1164 doi:10.1016/0016-7037(82)90246-0

1165 Kröner, A., 1977, The Precambrian geotectonic evolution of Africa: plate accretion vs.
1166 plate destruction: *Precambrian Research*, v. 4, p. 163–213.

1167 Kröner, A., Greiling, R., Reischmann, T., Hussein, I.R.M., Stern, R.J., Dürr, S., Kruger,
1168 J., and Zimmer, M., 1987, Pan-African crustal evolution in the Nubian segment of
1169 northeast Africa. *In* Kröner, A., ed., Proterozoic Lithosphere Evolution: American
1170 Geophysical Union Geodynamics Series, 17, (Washington D.C.) p. 235-257.
1171 <https://doi.org/10.1029/GD017p0235>

1172 Kröner, A., Pallister, J.S., and Fleck, R.J., 1992, Age of initial oceanic magmatism in the
1173 Late Proterozoic Arabian Shield: *Geology*, v. 20, p. 803–806.

1174 Landis, G.P., and Rye, R.O., 2005, Characterization of gas chemistry and noble-gas
1175 isotope ratios of inclusion fluids in magmatic-hydrothermal and magmatic-steam
1176 alunite: *Chemical Geology*, v. 215, p. 155– 184.

1177 Large R.R., Bull S.W., and Maslennikov, V.V., 2011, A carbonaceous sedimentary
1178 source-rock model for Carlin-type and orogenic gold deposits: *Economic Geology*,
1179 v. 106, p. 331–358.

1180 Large, R.R., Gregory, D.D., Steadman, J.A., Tomkins, A.G., Lounejeva, E.,
1181 Danyushevsky, L.V., Halpin, J.A., Maslennikov, V., Sack, P.J., Mukherjee, I.,
1182 Berry, R., and Hickman, A., 2015, Gold in the oceans through time: *Earth and*
1183 *Planetary Science Letters*, v. 428, p. 139-150. doi.org/10.1016/j.epsl.2015.07.026.

1184 Lowenstern, J.B., 2001, Carbon dioxide in magmas and implications for hydrothermal
1185 systems: *Mineralium Deposita*, v. 36, p. 490–502.

1186 Lüders, V., Klemd, R., Oberthür, T., and Plessen, B., 2015, Different carbon reservoirs of
1187 auriferous fluids in African Archean and Proterozoic gold deposits? Constraints
1188 from stable carbon isotopic compositions of quartz-hosted CO₂-rich fluid
1189 inclusions: *Mineralium Deposita*, v. 50, p. 449–454.

1190 Mavrogenes, J.A., and Bodnar, R.J., 1994, Hydrogen movement into and out of fluid
1191 inclusions in quartz: Experimental evidence and geologic implication: *Geochimica*
1192 *et Cosmochimica Acta*, v. 58, p. 141-148.

1193 Merdith, A.S., Collins, A.S., Williams, S.E., Pisarevsky, S., Foden, J.D., Archibald, D.B.,
1194 Blades, M.L., Alessio, B.L., Armistead, S., Plavsa, D., Clark, C., and Müller, R.D.,
1195 2017. A full-plate global reconstruction of the Neoproterozoic: *Gondwana*
1196 *Research*, v. 50, p. 84-134.

1197 Mumm, A.S., Oberthür, T., Vetter, U., and Blenkinsop, T.G., 1997, High CO₂ content of
1198 fluid inclusions in gold mineralisations in the Ashanti Belt, Ghana: A new category
1199 of ore forming fluids?: *Mineralium Deposita*, v. 32, p. 107–118. doi:
1200 10.1007/s001260050078.

1201 Perret, J., Eglinger, A., André-Mayer, A-S., Aillères, L., Feneyrol, J., Hartshorn, C.,
1202 Abanyin, E., and Bosc, R., 2020, Subvertical, linear and progressive deformation
1203 related to gold mineralization at the Galat Sufar South deposit, Nubian Shield, NE
1204 Sudan: *Journal of Structural Geology*, v. 135, 104032.
1205 doi.org/10.1016/j.jsg.2020.104032

1206 Phillips, G.N., and Powell, R., 1993, Link between gold provinces: *Economic Geology*,
1207 v. 88, p. 1084–1098. doi:10.2113/gsecongeo.88.5.1084.

1208 Phillips, G.N., and Powell, R., 2010, Formation of gold deposits: A metamorphic
1209 devolatilization model: *Journal of Metamorphic Geology*, v. 28, p. 689–718.
1210 doi:10.1111/j.15251314.2010.00887.x.

1211 Pitcairn, I.K., Olivo, G.R., Teagle, D.A.H., and Craw, D., 2010, Sulfide evolution during
1212 prograde metamorphism of the Otago and Alpine Schists, New Zealand: *Canadian*
1213 *Mineralogist*, v. 48, p. 1267–1295.

1214 Pitcairn, I.K., Craw, D., and Teagle, D.A.H., 2015, Metabasalts as sources of metals in
1215 orogenic gold deposits: *Mineralium Deposita*, v. 50, p. 373–390.

1216 Pohl, W. 1988, Precambrian metallogeny of Northeast-Africa, the Pan-African Belt of
1217 northeast Africa and adjacent areas. Friedrich Vieweg und Sohn,
1218 Braunschweig/Wiesbaden, 319–341p.

1219 Prokofiev, V.Y., and Naumov, V.B., 2020, Physicochemical Parameters and
1220 Geochemical Features of Ore-Forming Fluids for Orogenic Gold Deposits
1221 Throughout Geological Time: *Minerals*, 10(1), 50
1222 <https://doi.org/10.3390/min10010050>

1223 Ramsey, C.A., and Hewitt, A.D., 2005, A Methodology for Assessing Sample
1224 Representativeness: *Environmental Forensics*, v. 6, p. 71–75.

1225 Reeves, E.P., and Fiebig, J., 2020, Abiotic Synthesis of Methane and Organic
1226 Compounds in Earth's Lithosphere: *Elements*, v. 16, p. 25–31.
1227 doi.org/10.2138/gselements.16.1.25

1228 Ridley J.R., and Diamond L.W., 2000, Fluid chemistry of lode-gold deposits and
1229 implications for genetic models. In: Hagemann S.G., Brown P. (Eds.), Gold in
1230 2000. Reviews in Economic Geology. Society of Economic Geologists, Inc., v. 13,
1231 pp. 141-162.

1232 Rocci, G., 1965, Essai d'interprétation de mesures géochronologiques. La structure de
1233 l'Ouest africain : Sciences Terre Nancy, v. 10, p. 461–479.

1234 Robert, F., and Poulsen, K.H., 2001, Vein Formation and deformation in greenstone gold
1235 deposits: Reviews in Economic Geology, v. 14, p. 111-155.

1236 Robert, F., Boullier, A.-M., and Firdaus, K., 1995, Gold–quartz veins in metamorphic
1237 terranes and their bearing on the role of fluids in faulting: Journal of Geophysical
1238 Research, Solid Earth, v. 100, p. 12,861–12,879.

1239 Sadofsky, S.J., and Bebout, G.E., 2000, Ammonium partitioning and nitrogen-isotope
1240 fractionation among coexisting micas during high-temperature fluid-rock
1241 interactions: examples from the New England Appalachians: Geochimica et
1242 Cosmochimica Acta, v. 64, p. 2835-2849.

1243 Schandelmeier, H., Wipfler, E., Küster, D., Sultan, M., Becker, R., Stern, R.J., and
1244 Abdelsalam, M.G., 1994, Atmur-Delgo suture: A Neoproterozoic oceanic basin
1245 extending into the interior of northeast Africa: Geology, v. 22, p. 563–566.

1246 Steadman, J.A., Large, R.R., Blamey, N.J., Mukherjee, I., Corkrey, R., Danyushevsky,
1247 L.V., Maslennikov, V., Hollings, P., Garven, G., Brand, U., and Lécuyer, C. 2020,
1248 Evidence for elevated and variable atmospheric oxygen in the Precambrian:
1249 Precambrian Research, 105722, doi.org/10.1016/j.precamres.2020.105722.

1250 Stern, R.J., 1994, Arc Assembly and continental collision in the Neoproterozoic East
1251 African Orogen: Implications for the consolidation of Gondwanaland: Annual
1252 Reviews of Earth and Planetary Science, v. 22, p. 319-351. doi:10.1146/
1253 annurev.ea.22.050194.001535.

1254 Stern, R.J., and Johnson, P., 2010, Continental lithosphere of the Arabian Plate: A
1255 geologic, petrologic, and geophysical synthesis: Earth-Science Reviews, v. 101, p.
1256 29–67.

- 1257 Stern, R.J., Kroner, A., Manton, W.I., Reischmann, T., Ansour, M.M., and Ussein, I.M.H.,
1258 1989. Geochronology of the late Precambrian Hamisana shear zone, Red Sea Hills,
1259 Sudan and Egypt: *Journal of the Geological Society*, v. 146, p. 1017-1029.
- 1260 Stern, R.J., Nielsen, K.C., Best, E., Sultan, M., Arvidson, R.E., and Kröner, A., 1990,
1261 Orientation of late Precambrian sutures in the Arabian-Nubian Shield: *Geology*, v.
1262 18, p. 1103-1106.
- 1263 Stern, R.J., Johnson, P.R., Kröner, A., and Yibas, B., 2004, Neoproterozoic Ophiolites of
1264 the Arabian-Nubian Shield: *Developments in Precambrian Geology*, v. 13, p. 95-128.
- 1265 Tadesse, S., Milesi, J.P., and Deschamps, Y., 2003. Geology and mineral potential of
1266 Ethiopia: a note on geology and mineral map of Ethiopia: *Journal of African Earth*
1267 *Sciences*, v. 36, p. 273-313.
- 1268 Tarantola, A., Diamond, L.W., Stünitz, H., Thust, A., and Pec, M., 2012. Modification of
1269 fluid inclusions in quartz by deviatoric stress. III: Influence of principal stresses on
1270 inclusion density and orientation: *Contributions to Mineralogy and Petrology*, v.
1271 164, p. 537-550.
- 1272 Teklay, M., Kröner, A., Mezger, K., and Oberhänsli, R., 1998, Geochemistry, Pb-Pb
1273 single zircon ages and Nd-Sr isotope composition of Precambrian rocks from
1274 southern and eastern Ethiopia: implications for crustal evolution in East Africa:
1275 *Journal of African Earth Sciences*, v. 26, p. 207–227.
- 1276 Tomkins, A.G., 2010, Windows of metamorphic sulfur liberation in the crust:
1277 implications for gold deposit genesis: *Geochimica et Cosmochimica*, v. 74, p.
1278 3246–3259.
- 1279 Tomkins, A.G., 2013a, A biogeochemical influence on the secular distribution of
1280 orogenic gold: *Economic Geology*, v. 108, p. 193–197.
- 1281 Tomkins, A.G., 2013b, On the source of orogenic gold: *Geology*, v. 41, p. 1255–1256.
- 1282 Trench, A., and Groves, D., 2015, The Western Arabian-Nubian Shield: A Rapidly
1283 Emerging Gold Province: *SEG News Letter* 101, April 2015, pp. 1–16.
- 1284 Wang, Y., Wang, K., and Konare, Y., 2018, N₂-rich fluid in the vein-type Yangjingou
1285 scheelite deposit, Yanbian, NE China: *Nature Scientific Reports*, v. 8, Article
1286 number: 566. doi.org/10.1038/s41598-018-22227-7

- 1287 Wilkinson, J.J., 2001, Fluid inclusions in hydrothermal ore deposits: *Lithos*, v. 55, p.
1288 229–272.
- 1289 Wilkinson, B.H., and Kesler, S.E., 2007, Tectonism and Exhumation in Convergent
1290 Margin Orogens: Insights from Ore Deposits: *The Journal of Geology*, v. 115, p.
1291 611-627.
- 1292 Wu, Y.-F., Evans, K., Fisher, L.A., Zhou, M.-F Hu, S.-Y., Fougereuse, D., Large, R.R.,
1293 and Li, J.W., 2020, Distribution of trace elements between carbonaceous matter and
1294 sulfides in a sediment-hosted orogenic gold system: *Geochimica et Cosmochimica*
1295 *Acta*, v. 276, p. 345-362. doi.org/10.1016/j.gca.2020.03.006.
- 1296 Wyman, D.A., Cassidy, K.F., and Hollings, P., 2016, Orogenic gold and the mineral
1297 systems approach: resolving fact, fiction and fantasy: *Ore Geology Review*, v. 78,
1298 p. 322–335.
- 1299 Xue, Y., Campbell, I.H., Ireland, T.R., Holden, P., and Armstrong, R., 2013, No mass-
1300 independent sulfur isotope fractionation in auriferous fluids supports a magmatic
1301 origin for Archean gold deposits: *Geology*, v. 41, p. 791–794.
- 1302
- 1303 Yibas, B., Reimold, W.U., Anhaeusser, C.R., and Koeberl, C., 2003, Geochemistry of the
1304 mafic rocks of the ophiolitic fold and thrust belts of southern Ethiopia: constraints
1305 on the tectonic regime during the Neoproterozoic (900–700 Ma): *Precambrian*
1306 *Research*, v. 121, p. 157–183.
- 1307 Zhong, R., Brugger, J., Tomkins, A.G., Chen, Y., and Li, W., 2015, Fate of gold and base
1308 metals during metamorphic devolatilization of a pelite: *Geochim Cosmochim Acta*,
1309 v. 171, p. 338–352.
- 1310 Zoheir, B.A., 2008, Structural controls, temperature–pressure conditions and fluid
1311 evolution of orogenic gold mineralisation at the Betam mine, south Eastern Desert,
1312 Egypt: *Mineralium Deposita*, v. 43, p. 79-95.

1313

1314

1315 **Table and Figure captions**

1316

1317 Table 1. Fluid type established on the proportion of H₂O (mole %) and specific gas
1318 content.

1319

1320 Figure 1: Simplified regional geological map showing the interpreted limit of the Keraf
1321 suture zone, with the location of Figure 2, modified from Evuk et al. (2014) and
1322 Karmakar and Schenk (2015). The Hamisana shear zone location is from Stern
1323 et al. (1989). The inset shows the distribution of the Arabian-Nubian Shield.

1324

1325 Figure 2: Landsat 8 satellite image with the interpreted lineaments and intrusive bodies
1326 and the locations of the studied gold-bearing sites and deposits.

1327

1328 Figure 3. Characteristics of the gold deposits. A) Shallow-dipping S₁ fabric at the WG-03
1329 deposit. B) Crosscutting relationship between the hornblende-plagioclase S₁
1330 foliation (perpendicular to the core) cut by later biotite schistosity (parallel to the
1331 core), drill hole SCM-08 at 100 m, WG-03. C) Aspect of the S₂ schistosity at the
1332 surface of the WG-03 deposit. D) Late quartz vein within a normal shear zone,
1333 as indicated by the dragging of the S₁ foliation along the quartz vein, WG-03
1334 deposit. E) Dyke-hosted gold mineralization in the Central C04 deposit. The
1335 contacts of the felsic dyke are affected by reverse shearing. F) Gold
1336 mineralization in the UTM deposit, where the fault-fill quartz veins are hosted in
1337 a S₂ shallow-dipping reverse shear zone.

1338

1339 Figure 4. Map showing the structural settings, metamorphic facies and trends of gold-
1340 bearing structures for the various study sites. The interpreted geological features
1341 are from Figure 2: pink areas are interpreted intrusions and light brown lines are
1342 interpreted lineaments. The blue circles are enlarged area for highlighting the
1343 variation of the structural setting at the local scale. The kilometeric value is for
1344 the diameter of the circle.

1345

1346 Figure 5. Characteristics of the gold-bearing sites associated with reverse shear zones. A)
1347 CS fabric indicating reverse movement at the Yasmine site. Note the mined

1348 fault-fill gold-bearing veins parallel to the C-plane. B) Reverse shear-hosted
1349 gold-bearing quartz vein at the Yasmine site. C) CS fabric indicating a reverse-
1350 shear zone controlled by a mafic dyke contact at the Negeim artisanal mine.
1351 Note that the mafic dyke contains the S fabric and that the mined fault-fill gold-
1352 bearing veins (excavation) are parallel to the C-plane. D) Thick and laminated
1353 fault-fill vein hosted in the reverse-shear zone at the Negeim artisanal mine. E)
1354 S₁ foliation in amphibolite-facies rocks, refolded by reverse movement with
1355 boudinaged quartz veinlet in the axial plane at Shereik-118. Note the strong
1356 retrograde iron carbonate alteration manifested by the orange colour. F)
1357 Mineralized zone at WG-14 marked by quartz veining hosted in a strongly
1358 deformed shallow-dipping S₁ high-strain zone with strong iron carbonate
1359 alteration.

1360

1361 Figure 6. Characteristics of the gold sites associated with strike-slip and normal
1362 movements. A) Narrow quartz vein (excavated) located along the dextral
1363 sheared contact of a mafic dyke at the SW-2 site. B) Sinistral shearing along the
1364 contact between basaltic and volcanic-sedimentary rocks at Sajid, with the
1365 artisanal mining of a narrow quartz vein. Note the oblique extensional quartz
1366 vein (dashed red line) used to interpret the stress field and the strike-slip sinistral
1367 movement. C) Strongly deformed and gold-bearing volcanic-sedimentary
1368 horizon between massive basaltic rocks at Korup. D) CS fabric relationship
1369 indicating dextral movement at the SE site. The S fabric is developed within the
1370 dyke, where a narrow quartz vein follows the dyke contact (C fabric). E) Normal
1371 movement along a shear zone indicated by the CS fabric relationship, NW site.
1372 Note the excavated deformed boudins of gold-bearing quartz veins. F) Normal
1373 shear zone, as indicated by the dragging of the S₁ fabric (yellow line) hosting a
1374 gold-bearing quartz vein at Shereik-118.

1375

1376 Figure 7. Results of the fluid inclusion analysis by solid probe mass spectrometry. A)
1377 Logarithmic graph of mole % of volatile components for the analysed samples.
1378 Samples are grouped by the type of fluids established based on specific volatile

1379 contents and proportions and ordered according to the released total pressure
1380 (mbar). The total pressure corresponds to the quantity of volatiles released by
1381 fluid inclusion decrepitation in the sample during analysis. Red lettering
1382 indicates samples shown in Figure 8. B) Logarithmic graph of mole % of
1383 volatile components showing the ranges (maximum and minimum percentages)
1384 of volatile contents for the 6 types of fluids. Fluid types are colour-coded as
1385 detailed in A. The colour-coded dots in the 0% line indicate that at least one
1386 sample is devoid of corresponding volatiles.

1387

1388 Figure 8. Photomicrographs showing the petrographic characteristics used for defining
1389 the 3 groups of fluid inclusions for fluid types 1, 2, 3, 4, and 5. Note that for
1390 fluid type 5, which is devoid of water, fluid inclusions of group 1 (red arrow) are
1391 lacking or present in very low proportions. The Zerene Stacker software was
1392 used to enhance the focus.

1393

1394 Figure 9. Comparison of fluid type with structural setting (A) and metamorphic facies (B)
1395 on bubble charts. The size of the bubble is proportional to the number of gold-
1396 bearing sites having such characteristics, up to a maximum value of 11. For fluid
1397 type, nil refers to sample without gas released.

1398

1399 Figure 10. Spatial distribution of the various types of fluids. The interpreted geological
1400 features are from Figure 2. The dashed ovals are interpreted as NW-trending
1401 fields of fluids. Pink areas are interpreted intrusions and light brown lines are
1402 interpreted lineaments. The blue circles are enlarged area for highlighting the
1403 variation of fluid types at the local scale. The kilometric value is for the diameter
1404 of the circle.

1405

1406 Figure 11. Schematic geodynamic evolution of the central part of the KSZ, modified
1407 from Evuk (2013). The 550°C isograd, corresponding to the transition between
1408 the greenschist and amphibolite facies, is represented schematically to illustrate
1409 the fundamental role of metamorphism in generating gold-bearing fluids from

1410 organic-rich sedimentary rocks. A) Formation of a sedimentary basin with
1411 basaltic crust separating cratons under an extensional regime. B) Interpreted
1412 double subduction during the closing of the basin with the formation of
1413 limestone representing the top part of the stratigraphic sedimentary succession.
1414 C) Closing of the sedimentary basin with folding, thrusting, late strike-slip
1415 shearing and metamorphism of the organic-rich sedimentary rocks and
1416 generation of metamorphic fluids induced by rising metamorphic isograds. Gold
1417 deposits are formed by these metamorphic fluids (red arrows) within the
1418 volcanic-sedimentary rocks of the KSZ, as illustrated by the UTM deposit, as
1419 well as in adjacent cratons, as illustrated by WG-03 and Sajid.